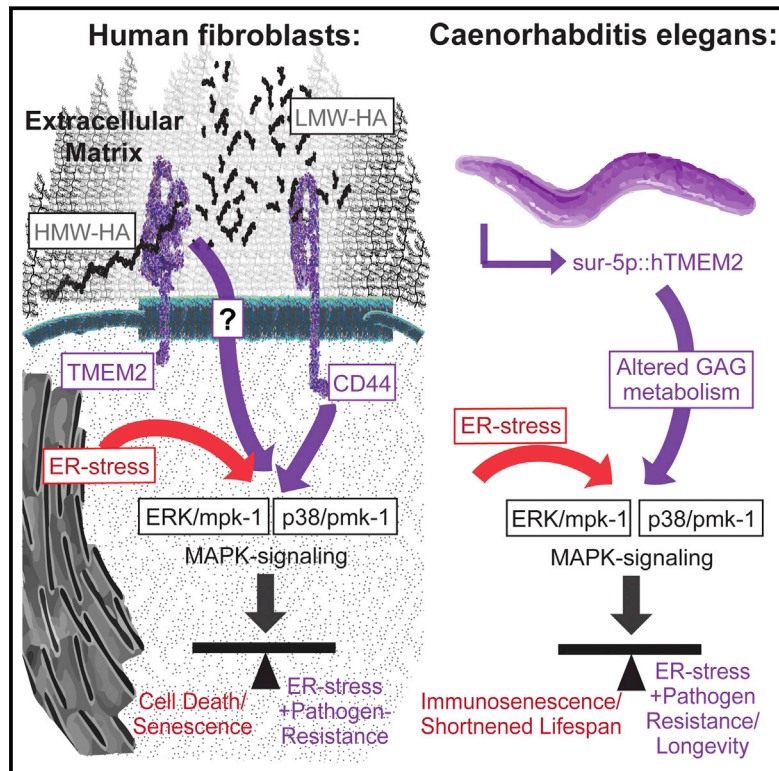# Cell

The Hyaluronidase, TMEM2, Promotes ER Homeostasis and Longevity Independent of the UPR^{ER}

Graphical Abstract

Authors

Robert Thomas Schinzel,
Ryo Higuchi-Sanabria, Ophir Shalem, ...,
Milos Simic, Ngoc-Tram Nguyen,
Andrew Dillin

Correspondence

dillin@berkeley.edu

In Brief

Intracellular ER stress resistance is impacted by changes in extracellular matrix metabolism.

Highlights

- CRISPR-Cas9 screening in human fibroblasts reveals TMEM2 as a regulator of ER stress

- TMEM2 alters intracellular ER stress resistance through changes in ECM metabolism

- TMEM2 promotes ER stress resistance independent of UPR^{ER} through MAPK signaling

- Ectopic expression of human TMEM2 promotes lifespan and immunity in *C. elegans*

CellPress

Article

Cell

The Hyaluronidase, TMEM2, Promotes ER Homeostasis and Longevity Independent of the UPR[ER]

Robert Thomas Schinzel,[1,2,3,5] Ryo Higuchi-Sanabria,[1,2,3,5] Ophir Shalem,[1,2,3,5,6] Erica Ann Moehle,[1,2,3]
Brant Michael Webster,[1,2,3] Larry Joe,[1,2,3] Raz Bar-Ziv,[1,2,3] Phillip Andrew Frankino,[1,2,3] Jenni Durieux,[1,2,3]
Corinne Pender,[1,2,3] Naame Kelet,[1,2,3] Saranya Santhosh Kumar,[4] Nupur Savalia,[1,2,3] Hannah Chi,[1,2,3] Milos Simic,[1,2,3]
Ngoc-Tram Nguyen,[1,2,3] and Andrew Dillin[1,2,3,7,*]

[1]Howard Hughes Medical Institute, University of California, Berkeley, Berkeley, CA 94720, USA
[2]California Institute for Regenerative Medicine, Berkeley, CA 94720, USA
[3]University of California, Berkeley, Berkeley, CA 94720, USA
[4]Center for Cellular and Molecular Therapeutics, Children's Hospital of Philadelphia, Philadelphia, PA 19104, USA
[5]These authors contributed equally
[6]Present address: Department of Genetics, Perelman School of Medicine, University of Pennsylvania, Pennsylvania, PA 19104, USA
[7]Lead Contact
*Correspondence: dillin@berkeley.edu
https://doi.org/10.1016/j.cell.2019.10.018

SUMMARY

Cells have evolved complex mechanisms to maintain protein homeostasis, such as the UPR[ER], which are strongly associated with several diseases and the aging process. We performed a whole-genome CRISPR-based knockout (KO) screen to identify genes important for cells to survive ER-based protein misfolding stress. We identified the cell-surface hyaluronidase (HAase), Transmembrane Protein 2 (TMEM2), as a potent modulator of ER stress resistance. The breakdown of the glycosaminoglycan, hyaluronan (HA), by TMEM2 within the extracellular matrix (ECM) altered ER stress resistance independent of canonical UPR[ER] pathways but dependent upon the cell-surface receptor, CD44, a putative HA receptor, and the MAPK cell-signaling components, ERK and p38. Last, and most surprisingly, ectopic expression of human TMEM2 in *C. elegans* protected animals from ER stress and increased both longevity and pathogen resistance independent of canonical UPR[ER] activation but dependent on the ERK ortholog *mpk-1* and the p38 ortholog *pmk-1*.

INTRODUCTION

In order to ensure the integrity of the proteome, eukaryotic organisms evolved distinct subcellular stress-response pathways, such as the unfolded protein response of the endoplasmic reticulum (UPR[ER]), the mitochondrial unfolded protein response (UPR[MT]), and the cytosolic heat shock response (HSR). These pathways induce transcriptional programs that allow cells to adapt to subcellular stress and promote cell survival. However, under severe and unmitigated proteotoxic stress, they are also central in triggering cellular senescence or programmed cell death through apoptosis (Hetz, 2012; Walter and Ron, 2011).

These challenges to the proteome can have a multitude of physiological and pathological causes. The ability to survive ER stress, for instance, is essential during the course of immune or inflammatory responses, during development, and cellular differentiation (Hetz, 2012; Wu and Kaufman, 2006). Additionally, ER stress is induced during intracellular pathogen replication, malignant cell growth, and the aging process (Hetz, 2009; Taylor and Dillin, 2013).

The induction of ER stress in both normal and pathophysiological contexts requires stress-response pathways to respond appropriately and flexibly based on the circumstances involved: the cell type affected, the nature of the challenge, and the severity and persistence of the assault (Chen and Brandizzi, 2013; Hetz, 2012; Sano and Reed, 2013; Xu et al., 2005). Central to UPR[ER] activation are ER-localized transmembrane proteins, IRE1, PERK1, and ATF6 (Gardner et al., 2013; Ron and Walter, 2007). These proteins serve as stress receptors, able to detect the load of unfolded proteins in the lumen of the organelle. In the presence of excessive levels of unfolded proteins, they signal to the nucleus to elicit a cellular response that results in a reduction in protein synthesis and expansion of the capacity of the ER. These changes are mediated through downstream signaling components, such as XBP1 or eIF2α. If there is no resolution to ER stress, the UPR[ER] is also central to trigger cell death/senescence by influencing several MAPK signaling-mediated cell-fate decisions (Darling and Cook, 2014; Hotamisligil and Davis, 2016). The MAPK-signaling components, p38, ERK, and JNK, integrate signals from the UPR[ER], from other subcellular stress-response pathways, as well as other cell-signaling pathways, to initiate regulated cell death/senescence. This mechanism provides the cell with a certain flexibility in response to ER stress, allowing the modulation of cell-fate decisions based on internal and extracellular cues. While much research has focused on the UPR[ER] and its interaction with other stress-response pathways, little is known how changes in the cellular microenvironment influence cell-fate decisions or the aging process in the presence of ER stress. For

Cell

example, it is not well understood how or which signals p38 and JNK receive to modulate ER stress responses.

Alongside a chronic activation of the UPR^{ER}, many pathologies present with significant changes in their cellular microenvironment, such as an altered glycosaminoglycan composition of the extracellular matrix (ECM). For example, an altered response to ER stress along with changes to the composition of the glycosaminoglycan, hyaluronan (HA), in the ECM has been observed in a variety of chronic-inflammatory and autoimmune diseases, in a subset of neurodegenerative diseases, and several malignancies (Brown and Naidoo, 2012; Chanmee et al., 2016; Hull et al., 2015; Majors et al., 2003; Nagy et al., 2015b, 2015a; Papy-Garcia et al., 2011). The polymer HA is a central component of the ECM and serves a variety of functions, such as basic structure, receptor protein attachment, and cell-to-cell communication (Cyphert et al., 2015; Laurent et al., 1996). The degradation of HA by enzymes, oxidative stress, and mechanical forces creates a continuum of different-sized HA fragments ranging from several oligosaccharides to molecules of over 1 million Daltons in size. Different sizes of HA possess distinct biological effects and changes in the size distribution of HA in the ECM have been found to induce cell-signaling pathways (Cyphert et al., 2015). Recently, transmembrane protein 2 (TMEM2) has been identified as a cell-surface hyaluronidase (HAase) able to break down high-molecular-weight HA (HMW-HA) into low-molecular-weight HA (LMW-HA) (De Angelis et al., 2017; Yamamoto et al., 2017).

This complexity and significance of the cellular stress-response pathways in the context of health and aging of an organism make protein quality-control mechanisms central to our understanding of several diseases (Hetz, 2012; Wang and Kaufman, 2012). While these pathways have been extensively studied in yeast and other model organisms, studies in the mammalian background have been more limited (Adamson et al., 2016; Horlbeck et al., 2018; Wang et al., 2014). Moreover, large-scale approaches almost always involved the use of cell lines derived from malignant cell growth, which often exhibit a severe dysregulation of stress-response pathways, thus impeding our understanding of biological function under non-cancerous conditions (Hanahan and Weinberg, 2011; Hetz, 2009). We therefore turned to the karyotypical stable human fibroblast for our research. Within this experimental model, we used pooled CRISPR libraries to perform whole-genome functional knockout (KO) screens in order to identify novel candidate genes and pathways that influence the response of cells to ER stress. Once identified, we tested their relevance *in vivo* using the nematode, *C. elegans*.

RESULTS

We performed a whole-genome CRISPR KO screen using the AVANA pooled single-guide RNA (sgRNA) library, with the aim of identifying genes, that, when inactivated, sensitized cells to ER stress (Figure 1A) (Doench et al., 2016; Shalem et al., 2014). Human immortalized fibroblasts were exposed to Tunicamycin, a drug that generates ER stress by inhibiting N-linked glycosylation, at a concentration that still maintained cell proliferation (Figure S1A). As non-transformed fibroblasts are not

commonly used for CRISPR screens, we verified our experimental system by testing the extent of essential gene depletions compared to other published datasets and found comparable quantitative depletion of essential genes (Figure S1B). Next, to identify gene KOs that selectively sensitize cells to ER stress, we compared gene-based depletion p values (see STAR Methods) between the control and treatment arms and restricted our analysis to genes that do not show any depletion in the control arm (Figure 1B). This approach identified the main components of the UPR^{ER}, IRE1, XBP-1, and PERK, as some of the most selectively depleted genes. The approach was further validated by identifying the gene, MFSD2A, a putative transporter required for Tunicamycin entry into the cells, as the most significantly enriched genetic ablation in the presence of Tunicamycin (Reiling et al., 2011). A second independent screen replicate showed highly reproducible results (Figure S1C). We then combined the two replicates to produce a final list of genes, which are either selectively enriched or depleted in response to Tunicamycin-induced ER stress (Table S1). An enrichment analysis of the significantly depleted genes revealed functions associated with ER protein processing, peroxisome, and additional related pathways (Figure 1C) (Chen et al., 2013; Kuleshov et al., 2016).

Among the most significantly depleted genes, in addition to the known members of the ER stress pathways, was Transmembrane Protein 2 (TMEM2) (Figure 1B). TMEM2 is localized to the plasma membrane, functions as a HAase within the ECM, and has not been previously implicated in ER stress, making it a prime candidate for further investigation.

TMEM2 Is Necessary and Sufficient for Regulating ER Stress Resistance

To verify the role of TMEM2 in ER stress regulation, we generated a clonal TMEM2-KO cell line (Figure S1D). TMEM2-KO cells had a significant decrease in resistance toward ER stress induced by either Tunicamycin or dithiothreitol (DTT) (Figures 1D and S1E). The re-introduction of wild-type TMEM2 expressed under a strong constitutive promotor (cytomegalovirus [CMV]) was able to rescue the ER stress sensitive phenotype of the TMEM2 KO cells (Figure 1D). In addition, ectopic expression of TMEM2 in non-mutated, wild-type cells also improved ER stress resistance (Figures 1D and S1E). We found no changes in cell proliferation in the absence of ER stress, resistance to mitochondrial stress (FCCP, carbonilcyanide p-triflouromethoxyphenylhydrazone), actin destabilizing compounds (Cytochalasin D), and cytoplasmic protein misfolding (sodium arsenite) between wild-type and TMEM2-KO cells (Figures S2A–S2D), suggesting that TMEM2's role in ER stress was specific. More importantly, these results indicate that TMEM2 is both necessary for protection toward ER stress and sufficient for protection toward ER stress when overexpressed.

The Hyaluronidase Activity of TMEM2, and Its Products, Is Responsible for ER Stress Protection in Human Fibroblasts

TMEM2 functions as a cell-surface HAase (De Angelis et al., 2017; Yamamoto et al., 2017). To determine whether the enzymatic breakdown of HA is responsible for the change in ER stress resistance, we generated several CMV-TMEM2
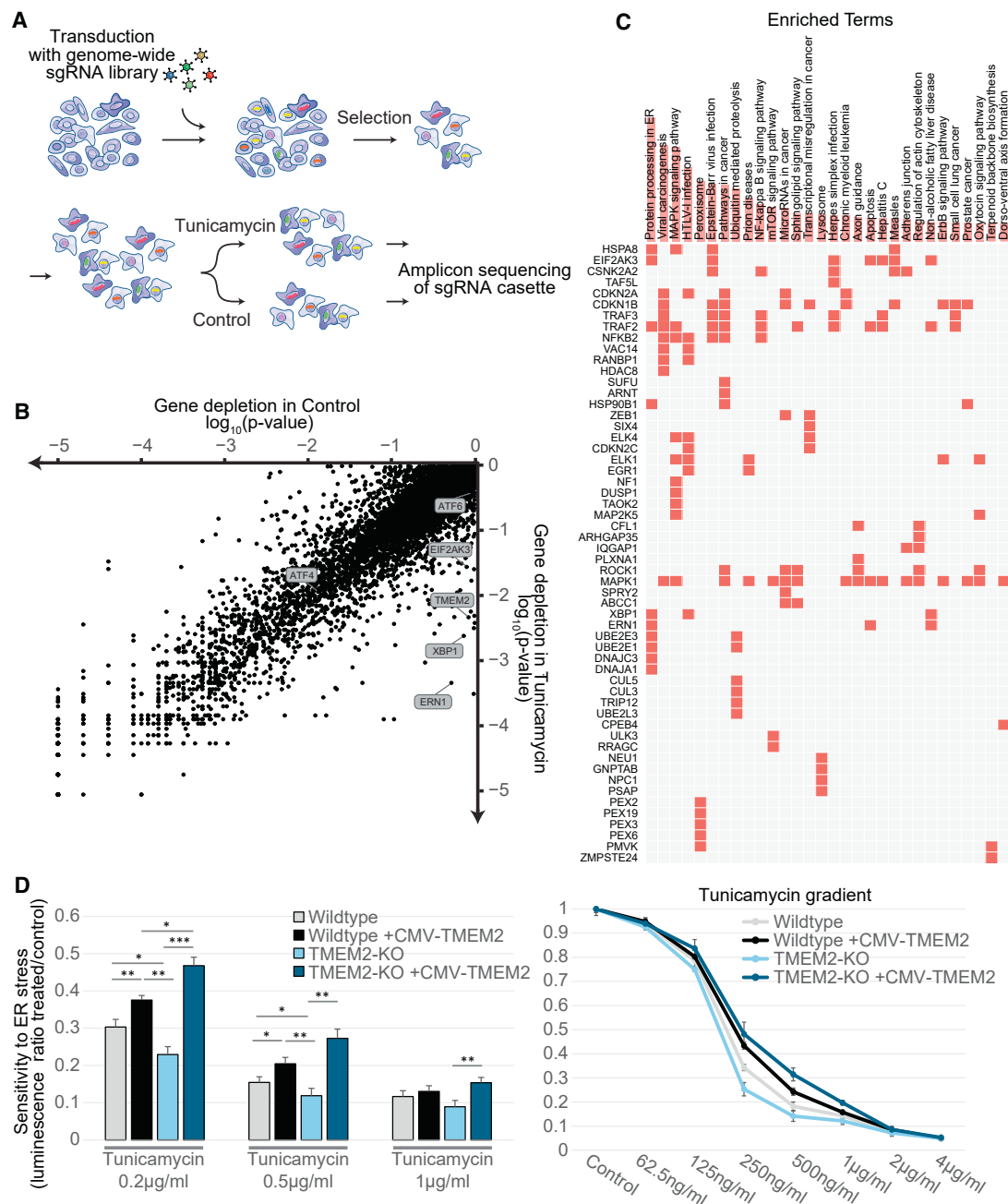
Figure 1. Whole-Genome CRISPR-KO Library Screen Identifies TMEM2 as a Potent Modulator of ER Stress Sensitivity

(A) Screen outline: human immortalized fibroblasts were transduced with a genome-wide sgRNA lentiviral library and cultured for 2 weeks to maximize genome editing and target protein depletion. Cells were then split into control and Tunicamycin treatment and harvested after 3 weeks of treatment for sequencing (as described in detail in STAR Methods).

(B) Comparison of gene depletion p values between control and Tunicamycin-treated cells (individual depletion/enrichment are available in Table S1).

(C) Enrichment analysis of the top differentially depleted genes (using 10% false discovery rate [FDR] as a cutoff) using the EnrichR online tool (https://amp.pharm.mssm.edu/Enrichr/).

(D) Viability and proliferation of wild-type and clonal TMEM2-KO human immortalized fibroblast in the presence of Tunicamycin-induced ER stress with or without CMV-TMEM2 overexpression.

Results are relative to untreated control to adjust for variability in initial cell number between cell lines. Cell density at the endpoint of a 5 day treatment period was determined via CellTiter-Glo analysis (CTG) (as described in detail in STAR Methods) (n = 3). Statistical analysis: one-way ANOVA analysis with post hoc Bonferroni-Holm analysis; * = $p < 0.05$; ** = $p < 0.01$, *** = $p < 0.001$. Bar graphs represent mean; all error bars for all plots represent standard deviation. See also Figure S1 and Table S1.
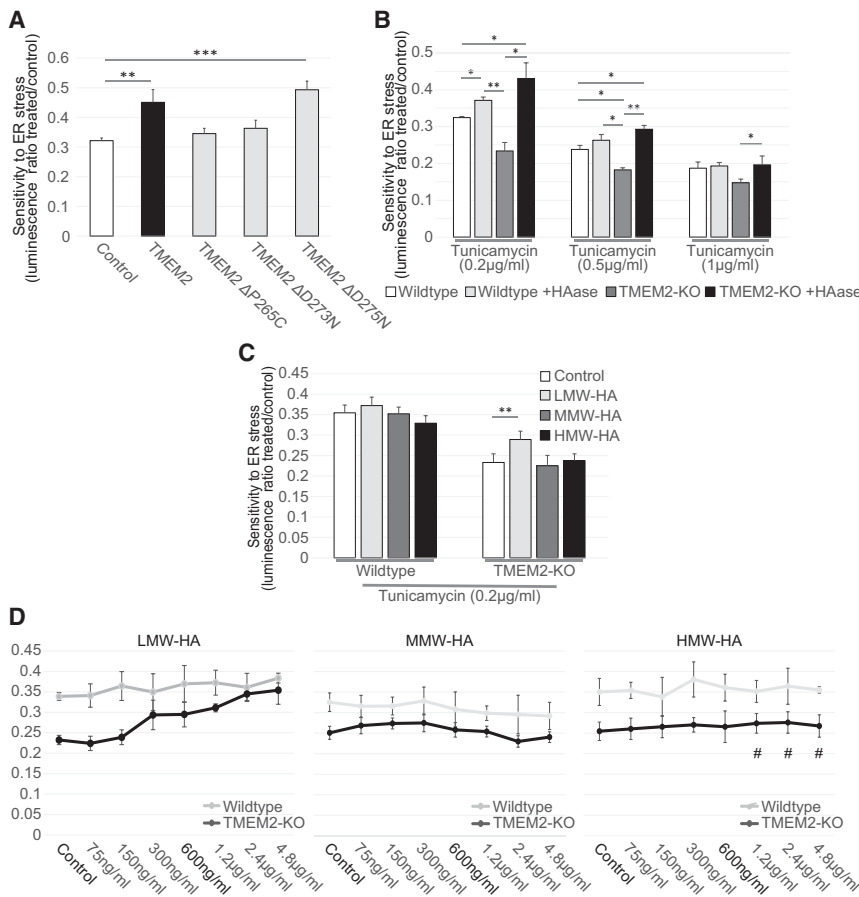
Cell

Figure 2. TMEM2's Enzymatic Breakdown of HMW-HA to LMW-HA Is Responsible for the ER Stress Phenotype

(A) The CMV-TMEM2 plasmid was altered through site-directed mutagenesis in order to disrupt HAase enzymatic activity of the gene. ER stress resistance was then measured through CTG analysis. The ER stress resistance was then compared between the constructs with no or a neutral mutation (ΔD275N) of the gene, and two lines in which the HAase function of TMEM2 was diminished (ΔP265C; ΔD273N) (n = 3).

(B) Resistance to Tunicamycin-induced ER stress was measured in wild-type and TMEM2-KO human fibroblasts in the presence and absence of supplemented HAase (concentration in bar graph: HAase 5 U/mL). All HAase concentrations tested (0.6–160 U/mL) were equally able to evoke this phenotype.

(C and D) Wild-type and TMEM2-KO cells were exposed to LMW-HA; <20 kDa in molecular weight, MMW-HA; 200–1,000 kDa, HMW-HA; >1,000 kDa. In (C), the concentration of LMW-HA, MMW-HA, and HMW-HA in the bar graphs represent 600 ng/mL of the compound. In (D), HMW-HA did not go fully into solution at concentrations higher than 600 ng/mL (marked with #). All bar graphs represent mean and * = p < 0.05; ** = p < 0.01, *** = p < 0.001. All error bars for all plots represent standard deviation. See also Figure S2.

TMEM2-KO cells in a concentration-dependent manner (Figures 2C and 2D). Therefore, the ER stress sensitivity in TMEM2-KO cells is not caused by a buildup of HMW-HA but rather by the lack of LMW-HA products produced by the HAase activity of TMEM2.

TMEM2-Mediated ER Stress Resistance Is Independent of the UPR^ER Pathways

A central response and driver of ER stress resistance is the activation of one of the three branches of the UPR^ER regulated by PERK1, ATF6, or IRE1. In order to test whether one of the three canonical UPR^ER branches was involved in the ER stress resistance conferred by TMEM2, we reduced the function of each branch of the UPR^ER and assessed ER stress resistance. We found that pharmacological inhibition of IRE1-dependent XBP1 splicing by the compounds, 4μ8C and STF-083010, did not impact the increased ER stress resistance observed in TMEM2-overexpressing cells nor did it influence the decreased ER stress sensitivity in TMEM2-KO cells (Figures 3A and S3A). Similarly, we observed no changes to stress resistance in the presence of the PERK1 inhibitor, GSK-2656157, or the downstream eIF2a inhibitor, Salubrinal (Figures 3B and S3B). We next targeted the three canonical UPR^ER branches, PERK1, ATF6, and IRE1, through CRISPR-mediated KO. Mutations within PERK1, ATF6, or IRE1 were not able to alter the TMEM2-KO phenotype or influence the ability to respond to HAase supplementation (Figure 3C). Last, we investigated whether TMEM2-KO human fibroblasts had an altered capacity

expression vectors in which the HAase function of TMEM2 was disrupted. Cells expressing enzymatic dead versions of TMEM2 failed to rescue the increased sensitivity to ER stress of TMEM2-KO cells (Figure 2A). However, a construct carrying a neutral mutation was able to rescue the phenotype, similar to the functional CMV-TMEM2 overexpression construct. Moreover, supplementation of the growth media with HAase enzyme derived from *Streptomyces hyalurolyticus* was also sufficient to rescue the stress sensitivity phenotype of the TMEM2 KO cells to wild-type levels and improved the resistance of wild-type cells, phenocopying the effect of TMEM2 overexpression (Figure 2B).

The HAase activity of TMEM2 is responsible for the breakdown of HMW-HA – above 1,000 kDa and moderate-molecular-weight HA (MMW – above 200 kDa, below 1,000 kDa) to LMW-HA – around 20 kDa in the ECM (De Angelis et al., 2017; Gialeli et al., 2014). Since different sizes of HA have been shown to possess distinct biological effects, we reasoned that the change in ER stress sensitivity of TMEM2 KO cells could be explained in two ways: either by the buildup of HA with a moderate to high molecular weight or the lack of LMW-HA (Cyphert et al., 2015). In order to explore these two possibilities, we supplemented HA of varying sizes to the growth media. We found that LMW-HA, but not MMW-HA or HMW-HA, was able to rescue the Tunicamycin sensitivity of
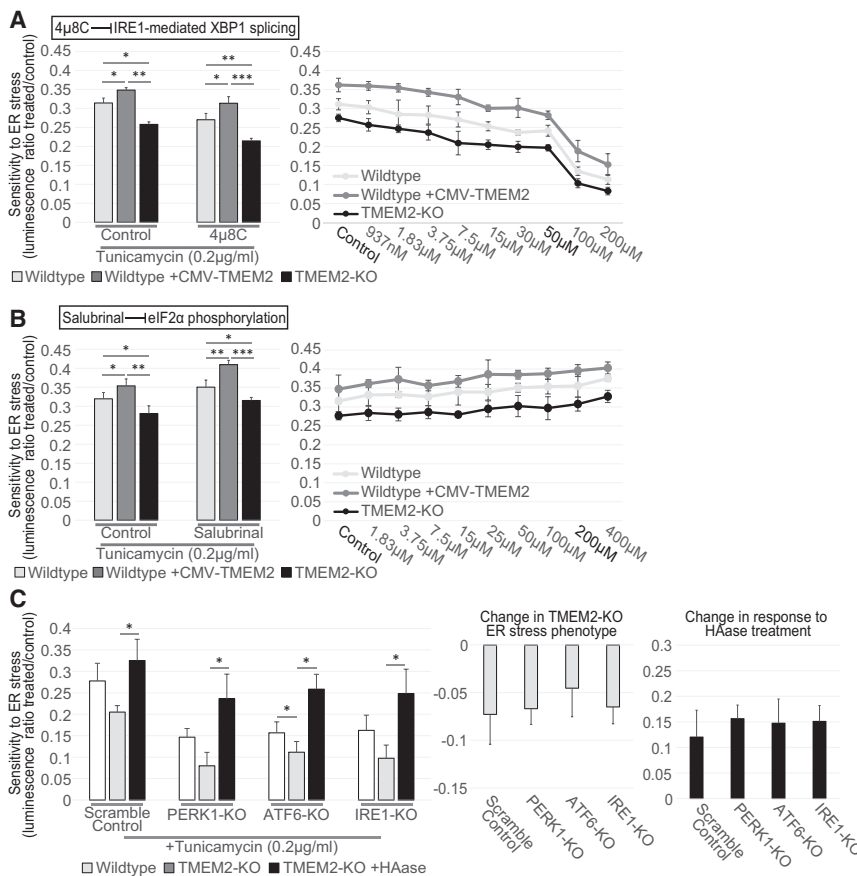
Cell

Figure 3. The TMEM2 ER Stress Phenotype Is Independent of the Three Canonical UPR^{ER} Pathways

(A and B) The resistance to Tunicamycin-induced ER stress of wild-type, TMEM2-KO, and CMV-TMEM2-overexpressing cells was determined in the presence of (A) an inhibitor of IRE1-mediated XBP1 splicing, 4μ8C (concentration in bar graphs: 4μ8C 50 μM; HAase 5 U/mL) or (B) an inhibitor of eIF2α phosphorylation, Salubrinal (concentration in bar graphs: Salubrinal 200 μM; HAase 5 U/mL) through CTG analysis (n = 3).

(C) In wild-type and TMEM2-KO cells, the UPR^{ER} pathway components IRE1, PERK1, and ATF6 were each targeted via CRISPR/CAS9-mediated gene disruption (see STAR Methods for details). Each cell line was then cultured in the presence and absence of Tunicamycin (200 ng/mL) and HAase (5 U/mL) for 5 days, and the cell density at the endpoint of the experiment was measured by CTG analysis (n = 3). The additional graphs highlight the on the TMEM2-KO ER stress phenotype and the response to HAase due to the targeting of the UPR^{ER} pathways.

Statistical analysis: one-way ANOVA analysis with post hoc Bonferroni-Holm analysis; * = p < 0.05; ** = p < 0.01, *** = p < 0.001. All bar graphs are represented as means. All error bars for all charts are standard deviations.See also Figures S3 and S4.

to induce the UPR^{ER} when exposed to Tunicamycin-induced ER stress by performing RNA sequencing (RNA-seq) analysis. Compared to wild-type cells, TMEM2-KO fibroblasts showed no significant difference in gene expression in response to ER stress both globally and specifically in UPR^{ER} target genes (Figure S4). Taken together, our data suggest that TMEM2 plays a unique role in ER stress resistance that is independent of the canonical pathways of PERK1, ATF6, and IRE1.

TMEM2 Mediates ER Stress Resistance through the CD44/ERK/p38 Pathway

In the presence of severe or unmitigated ER stress, mitotic cells respond by inducing apoptosis or cellular senescence. Previous work identified three MAPK pathway components as central in cell-fate decisions in the presence of ER stress: ERK, p38, and JNK (Darling and Cook, 2014; Sui et al., 2014). We therefore tested whether any of these MAPK pathways were involved in the TMEM2-associated changes in ER stress resistance. For this, we exposed the cells to the ERK inhibitor SCH772984, the p38 inhibitor SB202190, or the JNK inhibitor SP600125 and measured their impact on the TMEM2-mediated ER stress phenotype. Inhibition of either p38 or ERK suppressed the ER stress resistance of TMEM2-overexpressing cells or cells treated with HAase to wild-type levels (Figures 4A and 4B). In contrast, JNK inhibition had no effect (Figure 4C). While this set of inhibitors are commonly used in studying MAPK signaling, their spec-

ificity has been questioned (Bain et al., 2007, 2003). We therefore included an additional set of small molecule inhibitors for each pathway: DEL-22379 (ERK inhibitor), SB239063 (p38 inhibitor), and AEG 3482 (JNK inhibitor), which confirmed our original findings (Figures S5A–S5C).

These results suggest that altered ER stress resistance in TMEM2-overexpressing cells is mediated through ERK and p38, but not JNK MAPK signaling. Intriguingly, similar to the overexpression phenotype, the decreased resistance of TMEM2-KO cells is dependent on ERK and p38, but not JNK signaling (Figures 4A–4C). We therefore concluded that both the sensitivity to ER stress of TMEM2-KO cells and the ER stress resistance of TMEM2-overexpressing cells are mediated through ERK/p38 MAPK signaling pathways.

Phenotypes associated with TMEM2 activity have been shown to depend upon the VEGF-VEGFR-ERK signaling pathway (De Angelis et al., 2017). However, neither VEGF supplementation (up to 200 ng/mL) nor VEGFR receptor inhibition, using the compound SU5416, had an effect on ER stress resistance by either HAase supplementation or TMEM2 KO (Figures S3C and S3D). Besides VEGFR, LMW-HA fragments (around 5–20 kDa) have been shown to interact with several other cell-surface receptors (De Angelis et al., 2017; Joy et al., 2018; Misra et al., 2015; Taylor et al., 2014; Tolg et al., 2014). Three of these have additionally been associated with changes to MAPK signaling: CD44, RHAMM, and ICAM-1 (Joy et al., 2018; Vigetti et al., 2014, 2008). We performed targeted disruption of the genomic locus of each of the receptors and measured potential changes to the ER stress resistance phenotype. We found no significant
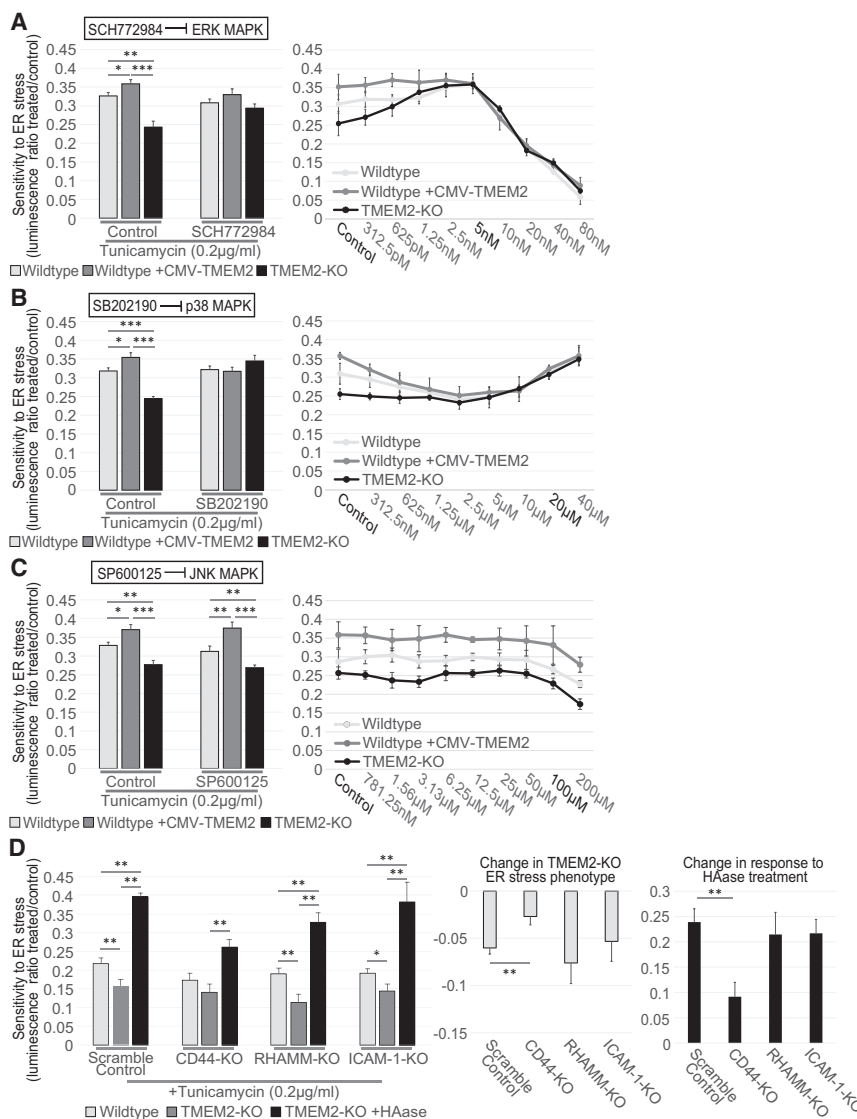
Cell

Figure 4. TMEM2 Mediates ER Stress Resistance through the MAPK Pathway Components, ERK and p38, and the Cell-Surface Receptor CD44

(A–C) ER stress resistance was measured in the presence of (A) the ERK inhibitor SCH772984 (concentration in bar graphs: SCH770984 5nM, HAase 5 U/mL), (B) the p38 MAPK pathway inhibitor SB202190 (concentration in bar graphs: SB202190 10 μM, HAase 5 U/mL), or (C) the JNK MAPK pathway inhibitor SP600125 (concentration in bar graphs: SP600125 5 μM, HAase 5 U/mL) (n = 3).

(D) In wild-type and TMEM2-KO cells, the cell-surface receptors CD44, RHAMM, and ICAM-1 were targeted via CRISPR/CAS9-mediated gene disruption (see STAR Methods for details). Each cell line was then cultured in the presence and absence of Tunicamycin (200 ng/mL) and HAase. ER stress resistance was measured through CTG analysis (n = 3). The additional graphs highlight the impact on the TMEM2-KO ER stress phenotype and the response to HAase due to the targeting of the receptors. Statistical analysis: one-way ANOVA analysis with post hoc Bonferroni-Holm analysis and * = p < 0.05; ** = p < 0.01, *** = p < 0.001. All bar graphs represent mean. All error bars for all plots represent standard deviation. See also Figures S4 and S5.

overexpression of the IRE1 pathway component, XBP-1 s is able to increase the lifespan and resistance to proteotoxic stress in several model organisms, such as *C. elegans* and *M. musculus* (Taylor et al., 2014; Taylor and Dillin, 2013; Williams et al., 2014).

To determine whether TMEM2 can play a similar role in abrogating age-associated decline in an animal's capacity to deal with ER stress, we used *C. elegans* as a model system to monitor the impact of TMEM2 expression upon aging. We introduced human TMEM2 (referred to as hTMEM2 in the context of *C. elegans* for clarity) into the worm using a pan-tissue promoter, *sur-5p*, and found that these animals were long-lived and protected from ER stress caused by Tunicamycin (Figures 5A and S6A). In an effort to determine whether hTMEM2 was necessary for these phenotypes in *C. elegans*, we identified the two closest nematode orthologs: *R07C12.1*, sharing a mere 30% identity based on amino acid sequence alignment, and *chhy-1*, the closest functional homolog (Csoka and Stern, 2013; Kaneiwa et al., 2008). We find that CRISPR-Cas9 KO of *R07C12.1* had no impact on longevity or stress resistance to Tunicamycin (Figure S6B). However, RNAi knockdown of *chhy-1* resulted in a significant decrease in lifespan and a very mild, but statistically significant, decrease in stress resistance to Tunicamycin, suggesting that there does exist some functional overlap between hTMEM2 and CHHY-1 and that *chhy-1* is necessary for a normal lifespan in *C. elegans*

difference in response to RHAMM or ICAM-1 deletion. However, deletion of CD44 reduced the differential stress resistance we found in TMEM2-KO cells and greatly reduced the response of the TMEM2-KO cells to HAase treatment (Figure 4D). Therefore, CD44 appears to be the likely receptor responsible for the changes in ER stress resistance caused by changes to HAase activity, consistent with CD44 being a possible receptor for HA.

Ectopic Expression of Human TMEM2 in *C. elegans* Results in Increased Lifespan, ER Stress Resistance, and Pathogen Resistance

Altered ER stress resistance impacts longevity in several animal models, including the nematode, *C. elegans*. Specifically, an animal's capacity to deal with ER stress decreases as a function of age, and hyperactivation of the ER stress response can ameliorate these defects, resulting in lifespan extension. The genetic activation of the UPR^ER through
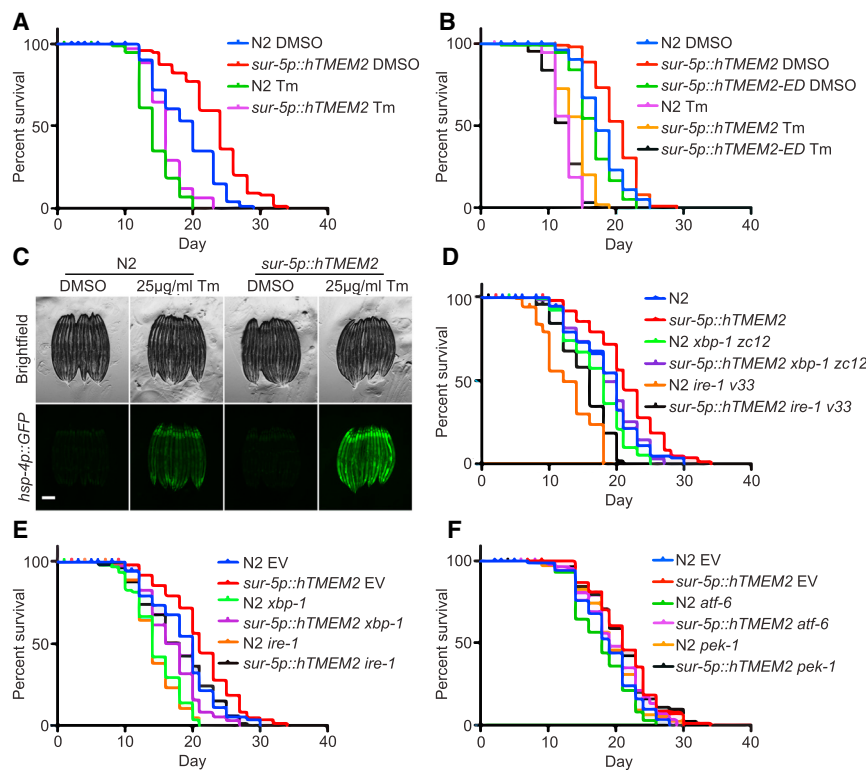
Cell

Figure 5. hTMEM2 Overexpression Extends Lifespan in _C. elegans_ Independent of Canonical UPR^ER Pathways

(A) Lifespans were measured in wild-type (N2) and _sur-5p::hTMEM2_ worms grown on empty vector (EV) RNAi on 1% DMSO and 25 μg/mL Tunicamycin (Tm) from day 1 (D1) as described in STAR Methods. Data are representative of four independent trials.

(B) Lifespans were measured in wild-type (N2), _sur-5p::hTMEM2_, and an enzymatic dead version of hTMEM2 (_sur-5p::hTMEM2-ED_, carrying R265C, D273N, D286N mutations; this overexpression line is an extrachromosomal array) using similar methods as in (A). Data are representative of three independent trials.

(C) Fluorescent micrographs of wild-type (N2) and _sur-5p::hTMEM2_ animals expressing the UPR^ER reporter, _hsp-4p::GFP_. Animals were treated with DMSO or 25 μg/mL Tunicamycin (Tm) at L4 and imaged at D1 as described in STAR Methods. Data are representative of four independent trials.

(D) Lifespans were measured in wild-type and _sur-5p::hTMEM2_ animals carrying either wild-type alleles of _xbp-1_ and _ire-1_ or mutant alleles, _xbp-1(zc12)_ or _ire-1(v33)_, on EV RNAi. Data are representative of three independent trials.

(E) Lifespans were measured in wild-type and _sur-5p::hTMEM2_ animals grown on EV, _xbp-1_, or _ire-1_ RNAi from hatch. Data are representative of three independent trials.

(F) Lifespans were measured in wild-type and _sur-5p::hTMEM2_ animals grown on EV, _atf-6_, or _pek-1_ RNAi from hatch. Data are representative of two independent trials. All statistics for lifespans were performed using log-rank (Mantel-Cox) test using PRISM and are available in Table S2. See also Figures S6 and S7.

(Figure S6C). Finally, to test whether hTMEM2-mediated lifespan extension and ER stress resistance is dependent on hTMEM2's enzymatic function, we overexpressed an enzymatic dead version of hTMEM2 (R265C, D273N, D286N, referred to as hTMEM2-ED) and found that hTMEM2-ED was not sufficient to extend lifespan or promote ER stress resistance (Figure 5B).

In our previous UPR^ER paradigm of longevity, _xbp-1 s_ overexpression in neurons (heretofore referred to as neuronal _xbp-1 s_) was sufficient to induce UPR^ER in distal tissue and extend lifespan (Taylor and Dillin, 2013). Therefore, we tested whether ectopic expression of hTMEM2 affected lifespan by activation of the UPR^ER, similar to overexpression of _xbp-1 s_. In contrast to our previous paradigm of longevity, overexpression of hTMEM2 throughout the animal did not activate the canonical UPR^ER in the absence of stress. However, it did result in increased UPR^ER induction in the presence of Tunicamycin (Figure 5C). To determine whether the physiological phenotypes of lifespan extension and ER stress resistance were dependent on canonical UPR^ER, similar to neuronal _xbp-1 s_, we performed lifespan experiments in the presence of RNAi against the major regulators of the UPR^ER. We find that hTMEM2 extended lifespan in worms harboring null mutations or RNAi knockdown of either _ire-1_ or _xbp-1_ (Figures 5D and 5E). Similarly, hTMEM2 extended lifespan in worms with RNAi knockdown of _pek-1_ (the _C. elegans_ ortholog of human PERK1) or _atf-6_, providing further evidence that the beneficial effects of hTMEM2 overex-

pression is not mediated through canonical UPR^ER (Figure 5F). Next, we tested the survival of animals with hTMEM2 overexpression when exposed to Tunicamycin at late age. Our previous work has reported that UPR^ER induction is lost at late age, resulting in increased sensitivity to ER stress (Taylor and Dillin, 2013). However, we find that hTMEM2-overexpressing animals still exhibit increased resistance to Tunicamycin even at late age when UPR^ER induction is completely abrogated (Figures S6D and S6E).

Next, we found that, unlike the _xbp-1 s_ paradigm, neuronal overexpression of hTMEM2 alone was not sufficient to extend lifespan or increase resistance to ER stress (Figure S6F). Last, we compared the transcriptome of both strains using RNA-seq. Neuronal _xbp-1 s_ animals globally induce canonical UPR^ER genes, while hTMEM2 animals fail to do so. A closer look at specific targets of _xbp-1 s_, such as _crt-1_, clearly show differences between these two lifespan extension paradigms (Figure S7). These data provide direct evidence that this longevity paradigm is distinct from previous ER stress-response paradigm involving _xbp-1 s_' role in UPR^ER and further confirms our findings in human cells.

TMEM2 Plays a Potent Role in Innate Immunity

During aging, _C. elegans_ become increasingly susceptible to bacterial infection, which is considered an important cause of death of the nematodes in old age (Zhao et al., 2017). A decline in _pmk-1_/p38 activity, as well as a decrease in UPR^ER activation,
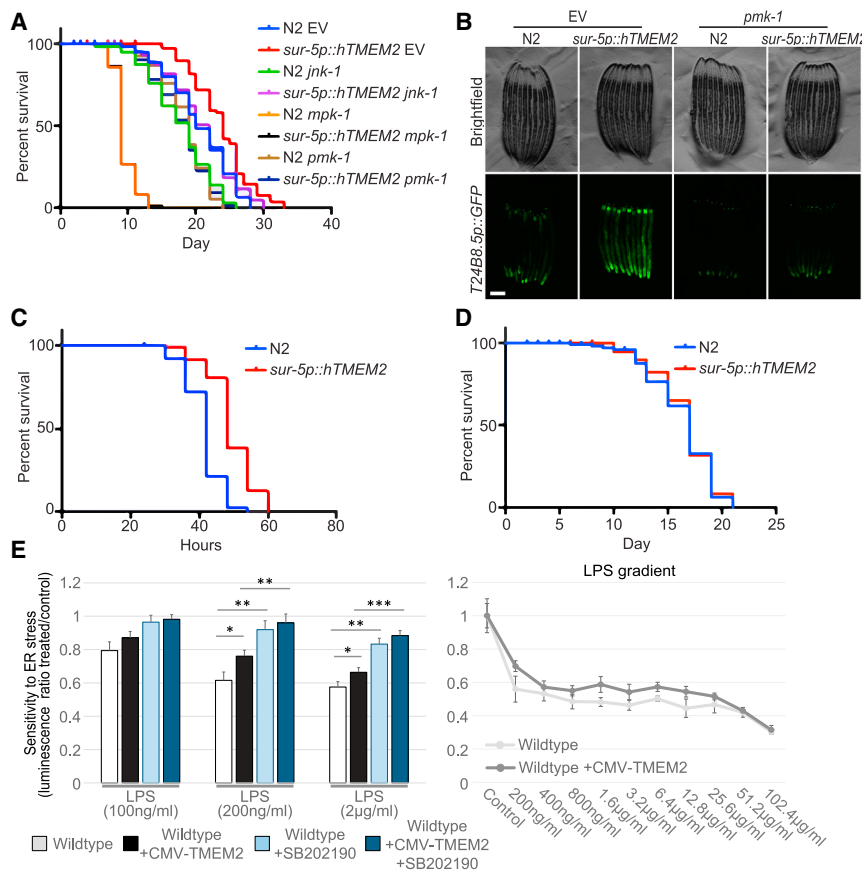
Cell

Figure 6. hTMEM2 Overexpression Promotes Immunity and Extends Lifespan through *mpk-1/pmk-1*

(A) Lifespans were measured in wild-type (N2) and *sur-5p::hsf-1* animals on EV, *jnk-1*, *mpk-1*, or *pmk-1* RNAi from hatch. Data are representative of three independent trials.

(B) Fluorescent micrographs of wild-type (N2) and *sur-5p::hTMEM2* animals expressing the immune response reporter, *T24B8.5p::GFP*. Animals were grown on EV or *pmk-1* RNAi as described in STAR Methods. Data are representative of three independent trials.

(C) Survival was scored in wild-type (N2) and *sur-5::hTMEM2* animals exposed to PA14 infection at L4. Survival was scored every 6 h as described in STAR Methods. Data are representative of two independent trials.

(D) Lifespans were measured in wild-type (N2) and *sur-5p::hTMEM2* animals grown on dead EV RNAi from hatch. Bacteria were killed by UV irradiation, as described in STAR Methods. All statistics for (C) and (D) were performed using log-rank (Mantel-Cox) test using PRISM and are available in Table S2.

(E) Wild-type and CMV-TMEM2-overexpressing human fibroblasts were exposed to lipopolysaccharides (LPSs) derived from the *E. coli* bacteria strain (O111:B4). Resistance to the presence of LPS was measured through CTG to determine the cell density after 5 days of exposure (n = 3). Statistical analysis: one-way ANOVA test with a post hoc Bonferroni-Holm analysis.

See also Table S2.

---

are central in this age-associated decline in innate immunity (Youngman et al., 2011). Moreover, we found in our human studies that loss of either ERK or p38 suppressed the beneficial effects of TMEM2. Therefore, we tested what role, if any, the ERK/p38 homologs, *mpk-1* or *pmk-1*, had on the beneficial physiological effects of hTMEM2 in *C. elegans*. Interestingly, we find that RNAi knockdown of *mpk-1* or *pmk-1* greatly suppressed the increased longevity of hTMEM2-overexpressing animals. Much like human cell studies, loss of *jnk-1* had no effect on hTMEM2 overexpression (Figure 6A). To directly test whether hTMEM2 activates immune response, we determined whether hTMEM2 can induce a reporter for the PMK-1 transcriptional target, *T24B8.5p::GFP* (Shivers et al., 2009). Indeed, we find that hTMEM2 induces this immune response reporter in a *pmk-1*-dependent manner (Figure 6B).

Next, we tested what role, if any, hTMEM2 could play in the survival of animals to the natural challenges of bacterial pathogens. We exposed hTMEM2 animals to the pathogenic bacteria, *Pseudomonas aeruginosa*, and measured their survival compared to control animals. hTMEM2 animals had a significantly higher resistance to the pathogen compared to controls (Figure 6C). Furthermore, when the worms were grown on *E. coli* bacteria previously killed through UV exposure, thus preventing bacterial infection, the difference in lifespan due to hTMEM2 overexpression was lost (Figure 6D). Therefore,

hTMEM2 plays an important role in the survival of cells and animals to pathogens.

In order to test whether a similar change in the response to pathogen plays a role in human fibroblasts overexpressing TMEM2, we exposed cells to lipopolysaccharides (LPSs) derived from the enteropathogenic *E. coli* strain (O111:B4). We found that overexpressing TMEM2 in fibroblasts abrogated the detrimental impact of LPS exposure compared to wild-type cells. The impact of LPS on both cell lines was entirely mediated through p38 MAPK signaling (Figure 6E).

Finally, we sought to determine whether the lifespan extension of neuronal *xbp-1 s* animals was also dependent on *mpk-1* and *pmk-1* signaling, similar to hTMEM2 overexpression. In contrast to hTMEM2-mediated lifespan extension, lifespan extension by neuronal *xbp-1 s* is completely independent of *jnk-1*, *mpk-1*, or *pmk-1* (Figure 7A). Moreover, neuronal *xbp-1 s* animals promotes lifespan extension when grown on bacteria previously killed through UV exposure (Figure 7B). Last, we find that neuronal *xbp-1 s* and hTMEM2 overexpression exhibits synergistic effects when combined (Figures 7C and 7D). Taken together, these data provide further evidence that neuronal *xbp-1 s* and hTMEM2 overexpression play independent and non-overlapping roles in lifespan extension where neuronal *xbp-1 s* modulates canonical UPR[ER] and hTMEM2 mediates innate immunity through *mpk-1* and *pmk-1*.
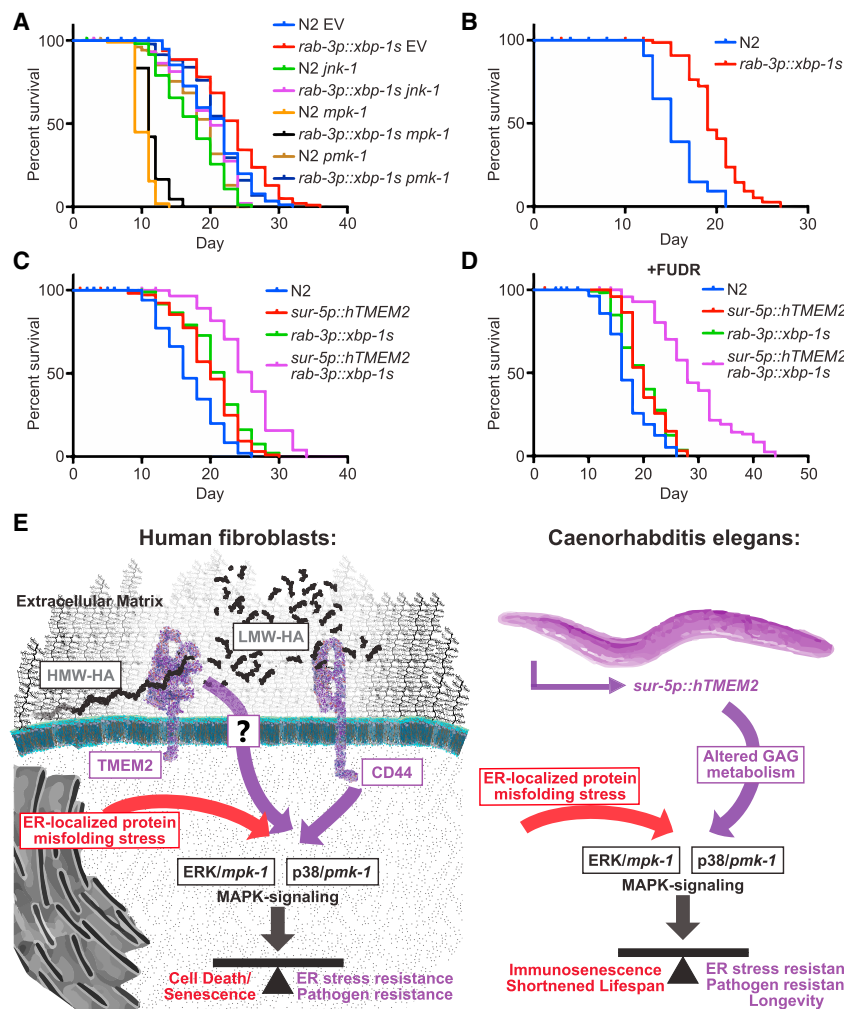
Cell

Figure 7. Lifespan Extension through Canonical *xbp-1 s* Signaling Is Not Dependent on *mpk-1/pmk-1* and Is Distinct from hTMEM2

(A) Lifespans were measured in wild-type (N2) and *rab-3p::xbp-1 s* animals on EV, *jnk-1*, *mpk-1*, or *pmk-1* RNAi from hatch. Data are representative of three independent trials.

(B) Lifespans were measured in wild-type (N2) and *rab-3p::xbp-1 s* animals grown on dead EV RNAi from hatch as per 5D. Data are representative of two independent trials.

(C and D) Lifespans were measured in wild-type (N2), *sur-5p::hTMEM2*, *rab-3p::xbp-1 s*, and *sur-5p::hTMEM2/rab-3p::xbp-1 s* animals in the absence (C) and presence (D) of FUDR (5-Fluoro-2′-deoxyuridine). Animals were grown on EV RNAi from hatch, and the assay was either performed on standard EV plates (C) or moved to FUDR containing plates at L4 for (D); see STAR Methods for details.

(E) Graphical representation of the key insight generated by this work. In human fibroblasts, TMEM2 breaks down HMW-HA into LMW-HA within the ECM. Through interaction with CD44, LMW-HA influences ERK/*mpk1-* and p38/*pmk-1*-mediated MAPK signaling. This in turn alters ER stress resistance and pathogen resistance in human fibroblasts. In *C. elegans*, TMEM2-mediated changes to glycosaminoglycan (GAG) metabolism cause a shift in MAPK signaling. This in turn alters the response to ER stress and, with it, changes pathogen resistance and the lifespan of the animals. See also Table S2.

senescence in mitotic cells (Chanmee et al., 2016; Chen and Brandizzi, 2013; Gerakis and Hetz, 2018; Hetz, 2012).

Since the vast majority of cells in the nematode, *C. elegans*, are post-mitotic after development, the lifespan extension is likely to be independent of an adjustment of programmed cell death. The central role of *pmk-1*/p38 activity in *C. elegans* involves innate immunity (Youngman et al., 2011). During aging, *C. elegans* exhibits tissue deterioration and an increased intestinal proliferation of bacteria, along with an increased susceptibility to bacterial infection. This susceptibility has been associated with a decline in *pmk-1*/p38 activity with increased age. The decline in innate immunity, generally referred to as innate immunosenescence, is considered an important cause of death of the nematodes in old age (Youngman et al., 2011; Zhao et al., 2017). Activation of ER stress responses have been shown to suppress immunity against bacterial pathogens and to contribute to immunosenescence (Singh and Aballay, 2006). The importance of cell survival under ER stress in the context of pathogen infection is also supported by the results of the whole-genome KO screen we performed in human fibroblast (Figures 1A and 1B). The enrichment analysis performed on the top, differentially deleted genes (sensitizers to ER stress), associated many of the genes as important factors in several different forms of pathogen infection.

DISCUSSION

We performed a genome-wide KO screen using pooled CRISPR libraries in karyotypical stable human fibroblasts to identify genes that mediate cell survival in the presence of ER stress. Through this approach, we were able to establish Transmembrane Protein 2 (TMEM2), a cell-surface hyaluronidase, as a potent modulator of ER stress resistance. TMEM2 activity is able to modulate ER stress resistance by altering the composition of the glycosaminoglycan HA in the ECM through enzymatic breakdown of HMW-HA to LMW-HA. The increase of the small metabolite LMW-HA ultimately alters the cell-fate decision in the presence of ER stress, through changes in p38/ERK MAPK signaling, mediated by the cell-surface receptor, CD44.

The ER stress response is thought to involve two stages. The first stage is characterized by a protective response that involves the expansion of the ER, induction of ER localized chaperones, and the reduction in protein load to the ER through decreased translation (Hetz, 2012; Wu and Kaufman, 2006). In the case of a persistent and unmitigated assault on the ER, the second phase involves the induction of apoptotic cell death or cellular

Cell

The expression of hTMEM2 in *C. elegans* was able to significantly increase the lifespan of animals and resistance to ER stress. This lifespan extension seems to follow different rules than the previously characterized *C. elegans* ER stress longevity model (Taylor and Dillin, 2013). Here, the selective expression of *xbp-1 s* in neurons of the nematode, extended the lifespan in an *xbp-1 s* and *ire-1*-dependent manner. Expression of *xbp-1 s* throughout the animal did not impact longevity. With hTMEM2, expression restricted to neurons is insufficient for the lifespan extension; rather, expression of hTMEM2 in all tissues is necessary to evoke the longevity phenotype. Furthermore, the lifespan extension is independent of *xbp-1* and *ire-1* in contrast to the *xbp1s* UPRER model. Last, in the UPRER longevity model, the expression of the ER localized chaperone, HSP-4, is significantly increased throughout the life of the animal. In the context of hTMEM2 expression, only changes to stress-induced *hsp-4* were observed in early adulthood.

One of the most surprising findings of this work is that TMEM2 regulates ER stress resistance independent of the UPRER. This was found in several ways. First, overexpression of TMEM2 protected wild-type human fibroblasts from ER stress in the presence of pharmacological inhibitors of XBP1, PERK1, and eIF2α. Second, genetic ablation of IRE1, PERK1, or ATF6 had no effect on the stress resistance phenotype mediated by TMEM2 in human cells or worms. Third, while overexpression of TMEM2 protected cells and worms from ER stress, it did not result in induction of the canonical UPRER target, HSPA5/*hsp-4*. Instead, TMEM2 links the small metabolite LMW-HA to CD44 and MAPK signaling through ERK and p38 signaling to protect cells from the damages of ER stress.

Why then has TMEM2 been missed in the plethora of discoveries surrounding ER stress resistance? The main reason for the lack of insight into TMEM2's role in ER stress could be that most studies in this field have focused on the transcriptional output of the response, in which TMEM2 has no role in. Indeed, the RNA-seq analysis of TMEM2 KO cells exposed to Tunicamycin showed little difference in the gene expression response compared to wild-type cells (Figures S4A–S4D). This indicates that TMEM2-KO cells are perfectly capable of inducing the full extent of the UPRER.

Similarly, our RNA-seq data comparing hTMEM2-overexpressing animals and neuronal *xbp-1 s* animals showed that, unlike neuronal *xbp-1 s* animals, hTMEM2 overexpression does not activate canonical UPRER targets. Moreover, *xbp-1 s*-mediated lifespan extension is independent of *pmk-1*/p38 and *mpk-1*/ERK. Finally, these two lifespan extension paradigms have synergistic effects, as animals with simultaneous neuronal *xbp-1 s* and hTMEM2 overexpression exhibit more than double the lifespan extension of either paradigm independently. Based on the results presented here, we propose that hTMEM2 overexpression in *C. elegans*, rather than by altering the UPRER directly, conveys longevity through changes to the *pmk-1*/p38 signaling pathway. This in turn alters how they adapt their cell fate in the presence of ER stress, ultimately prolonging the lifespan of the animals by delaying immunosenescence (Youngman et al., 2011). This suggests that rather than by altering the initial, protective stage of the response to ER stress, the longevity phenotype we observe in the presence of hTMEM2 overexpression would be due to changes of the second stage of the response, through the avoidance of the detrimental consequences of ER stress, specifically its impact on innate immunity.

The effects of hTMEM2 on *C. elegans* ER stress resistance and longevity are also surprising since the main structural glycosaminoglycan utilized by the animal is Chondroitin, and the presence of HA is disputed (Csoka and Stern, 2013; Yamada et al., 2011). We provide evidence that hTMEM2's enzymatic function is critical for its effect on ER stress resistance and longevity and that there is a striking conservation of the phenotypes and cellular signaling mechanisms involved across species. Furthermore, supplementation of HA to the animals caused a substantial developmental perturbation and alterations in sex determination in *C. elegans* (data not shown). While these results point to the role of HA metabolism in the nematode biology, alternative explanations are plausible. Most prominently, hTMEM2 could potentially serve as a Chondroitinase in the nematode. Supporting this reasoning is the structural similarity of Chondroitin and HA, the conservation of the functional domains of both enzyme families, and the previously observed considerable overlap of substrate specificities of both HAase and Chondroitinase enzymes (Csoka and Stern, 2013; Wang et al., 2017). Unfortunately, due to a range of experimental constraints, our attempts to distinguish between these two possibilities were not successful. We can therefore only come to the more general conclusion that the effects of hTMEM2 in *C. elegans* is likely due to changes in glycosaminoglycan metabolism. However, the impact of hTMEM2 expression on *mpk-1*/*pmk-1* MAPK signaling solidify an important contribution for this enzyme and the downstream signaling pathway in ER stress resistance and longevity.

In human fibroblast, the results of our experiments strongly implicate a shift of HA metabolism as the driver of the TMEM2-mediated shift in ER stress resistance. HAase supplementation phenocopies the effect of TMEM2 overexpression, while LMW-HA supplementation rescues defects in TMEM2-KO. Our data strongly implicate CD44/LMW-HA interaction as an important factor for the shift in ER stress resistance in human cells. These experiments nonetheless leave room for the possibility that CD44 is not the sole LMW-HA-receptor responsible, nor can they completely rule out a role for Chondroitin metabolism in the phenotypes we observed. Furthermore, since both Chondroitin and HA serve as an attachment point for a variety of cell-surface receptors, changes to glycosaminoglycan composition in the ECM might also impact receptor abundance on the cell surface more generally and additional confounding interactions are plausible.

There are several physiological conditions that are known to cause a degradation of glycosaminoglycans within the cellular microenvironment, including an exposure to oxidative stress, mechanical forces, and enzymatic breakdown through bacterial pathogens and leukocytes. The involvement of the ECM and cell-surface receptors in the modulation of ER stress resistance we described here, would therefore allow the cell to integrate extracellular signals from the prevailing microenvironment to the response to intracellular protein-folding perturbations. The fragmentation of glycosaminoglycans in the ECM in this context can be seen as an extracellular cue that adjust the cell-fate

Cell

decision of cells experiencing cellular stress, such as the presence of pathogens or the activation of an immune response.

An increase in ER stress, changes to the ECM, as well an altered MAPK signaling have all been identified as characteristic cellular phenotypes in tissues undergoing age-associated decline (Brown and Naidoo, 2012; Kurz and Tan, 2004; Morawski et al., 2014; Robert and Labat-Robert, 2015; Tigges et al., 2014). Similarly, the pathology of multiple diseases, ranging from a subset of neurodegenerative diseases, autoimmune and inflammatory diseases, and several malignancies show similar characteristic pathophysiological changes to the ECM, MAPK signaling, and signs of a prolonged exposure to ER stress (Gerakis and Hetz, 2018; Kim and Choi, 2010; Morawski et al., 2014; Robert and Labat-Robert, 2015; Robertson, 2016; Sherman et al., 2015). In many of these diseases, age is an important risk factor. Taken together, a loosely framed network of TMEM2, HA, cell-surface receptors, and p38/ERK can be created that could serve as an explanatory model in how these factors contribute to age-associated decline and disease etiology. Furthermore, our work introduces an additional mechanisms of how age-associated changes to ER stress levels and ECM composition influence pathogenesis.

Besides an opportunity to illuminate new disease mechanisms, our work might serve to inform therapeutic interventions, be it through changes in ECM composition or cellular signaling. That a modification of this network is in principle possible, is suggested by experimental results in another longevity model organisms in which HA plays an important part, the naked mole rat (NMR). The NMR is the longest living rodent species and seems almost completely resistant to cancer. This resistance is thought to be caused by a high abundance of HA with up to 5 times higher molecular weight, partly due to an increase in HA synthesis through HAS2 (HA synthase) and due to lowered activity of HA enzymatic breakdown (HYAL2). The abundance and composition of HA seems to be at the root of the resistance to malignant transformation, since either knocking down HA synthesis or overexpression of the HA-degrading enzyme, HYAL2, caused NMR fibroblast to become susceptible to malignant transformation (Tian et al., 2013). These results, along with the insights presented here, strongly suggest that at least part of the cancer resistance is due to a decreased resistance to ER stress. This line of reasoning is supported by the observation that fibroblasts from NMR show an increase in ER stress sensitivity, further highlighting the interconnection of ER stress resistance to the abundance and enzymatic breakdown of HA (Salmon et al., 2008). However, in contrast to our hTMEM2-overexpression model in *C. elegans*, the NMR is long lived while at the same time exhibits generally reduced HAase activity. This might be explained by the observation that cells of the NMR are more responsive to some types of HA signaling, compared to other mammalian cells (Tigges et al., 2014). Understanding the unique molecular mechanism underlying the different animal and human cell-culture models could therefore provide the opportunity to manipulate these pathways independently, thereby guiding the development of novel therapeutic interventions.

Last is a cautionary note. HA is increasingly used as a growth matrix to grow cells *in vitro*, and HAase enzymatic breakdown of the matrix is utilized to dissociate the cells from the culture dish.

We would like to point out that the biological activity of the HA fragments generated in this process might interfere with experimental results, especially in the context of studying cellular stress.

STAR★METHODS

Detailed methods are provided in the online version of this paper and include the following:

- KEY RESOURCES TABLE
- LEAD CONTACT AND MATERIALS AVAILABILITY
- EXPERIMENTAL MODEL AND SUBJECT DETAILS
  - *C. elegans* growth and maintenance
  - Cell culture and maintenance of human fibroblasts
  - Cell counting
- METHOD DETAILS
  - *C. elegans* induction of ER stress and immune response reporter
  - *C. elegans* lifespan measurements
  - *C. elegans* RNA-seq and analysis
  - CellTiter-Glo® luminescence viability assay
  - Clonal expansion
  - Clonal expansion of TMEM2 and control lines
  - CRISPR/CAS9-mediated gene disruption
  - Genomic DNA extraction and screen library preparation
  - Human Fibroblast RNaseq and analysis
  - Lentiviral production and transduction of expression vectors in general
  - Library lentiviral production
  - Screen cell culture
  - Screening data analysis
- QUANTIFICATION AND STATISTICAL ANALYSIS
- DATA AND CODE AVAILABILITY

AUTHOR CONTRIBUTIONS

R.T.S., O.S., and A.D. were involved in conceptualization. R.T.S. and O.S. performed the KO screens. O.S. was responsible for the data analysis of the screen. R.T.S. designed, performed, and analyzed the cell-culture experiments, with the help of O.S., E.A.M., P.A.F., N.S., and H.C. Important experimental resources were provided by R.T.S., O.S., R.H.-S., E.A.M., B.M.W., M.S., and P.A.F. R.H.-S. designed and performed *C. elegans* strain

Cell

DECLARATION OF INTERESTS

REFERENCES

Adamson, B., Norman, T.M., Jost, M., Cho, M.Y., Nuñez, J.K., Chen, Y., Villalta, J.E., Gilbert, L.A., Horlbeck, M.A., Hein, M.Y., et al. (2016). A Multiplexed Single-Cell CRISPR Screening Platform Enables Systematic Dissection of the Unfolded Protein Response. Cell *167*, 1867–1882.

Anders, S., and Huber, W. (2010). Differential expression analysis for sequence count data. Genome Biol *11* (10), 106.

Bain, J., McLauchlan, H., Elliott, M., and Cohen, P. (2003). The specificities of protein kinase inhibitors: an update. Biochem. J. *371*, 199–204.

Bain, J., Plater, L., Elliott, M., Shpiro, N., Hastie, C.J., McLauchlan, H., Klevernic, I., Arthur, J.S.C., Alessi, D.R., and Cohen, P. (2007). The selectivity of protein kinase inhibitors: a further update. Biochem. J. *408*, 297–315.

Brown, M.K., and Naidoo, N. (2012). The endoplasmic reticulum stress response in aging and age-related diseases. Front. Physiol. *3*, 263.

Chanmee, T., Ontong, P., and Itano, N. (2016). Hyaluronan: A modulator of the tumor microenvironment. Cancer Lett. *375*, 20–30.

Chen, Y., and Brandizzi, F. (2013). IRE1: ER stress sensor and cell fate executor. Trends Cell Biol. *23*, 547–555.

Chen, E.Y., Tan, C.M., Kou, Y., Duan, Q., Wang, Z., Meirelles, G.V., Clark, N.R., and Ma'ayan, A. (2013). Enrichr: interactive and collaborative HTML5 gene list enrichment analysis tool. BMC Bioinformatics *14*, 128.

Csoka, A.B., and Stern, R. (2013). Hypotheses on the evolution of hyaluronan: a highly ironic acid. Glycobiology *23*, 398–411.

Cyphert, J.M., Trempus, C.S., and Garantziotis, S. (2015). Size Matters: Molecular Weight Specificity of Hyaluronan Effects in Cell Biology. Int. J. Cell Biol. Published online September 10, 2015. https://doi.org/10.1155/2015/563818.

Darling, N.J., and Cook, S.J. (2014). The role of MAPK signalling pathways in the response to endoplasmic reticulum stress. Biochim. Biophys. Acta *1843*, 2150–2163.

De Angelis, J.E., Lagendijk, A.K., Chen, H., Tromp, A., Bower, N.I., Tunny, K.A., Brooks, A.J., Bakkers, J., Francois, M., Yap, A.S., et al. (2017). Tmem2 Regulates Embryonic Vegf Signaling by Controlling Hyaluronic Acid Turnover. Dev. Cell *40*, 421.

Dobin, A., Davis, C.A., Schlesinger, F., Drenkow, J., Zaleski, C., Jha, S., Chaisson, M., Gingeras, T.R., and Batut, P. (2013). STAR: ultrafast universal RNA-seq aligner. Bioinformatics *29*, 15–21.

Doench, J.G., Fusi, N., Sullender, M., Hegde, M., Vaimberg, E.W., Donovan, K.F., Smith, I., Tothova, Z., Wilen, C., Orchard, R., et al. (2016). Optimized sgRNA design to maximize activity and minimize off-target effects of CRISPR-Cas9. Nat. Biotechnol. *34*, 184–191.

Eden, E., Lipson, D., Yogev, S., and Yakhini, Z. (2007). Discovering motifs in ranked lists of DNA sequences. PLoS Comput. Biol. *3*, e39.

Eden, E., Navon, R., Steinfeld, I., Lipson, D., and Yakhini, Z. (2009). GOrilla: a tool for discovery and visualization of enriched GO terms in ranked gene lists. BMC Bioinformatics *10*, 48.

Gardner, B.M., Pincus, D., Gotthardt, K., Gallagher, C.M., and Walter, P. (2013). Endoplasmic reticulum stress sensing in the unfolded protein response. Cold Spring Harb. Perspect. Biol. *5*, a013169.

Gerakis, Y., and Hetz, C. (2018). Emerging roles of ER stress in the etiology and pathogenesis of Alzheimer's disease. FEBS J. *285*, 995–1011.

Gialeli, Ch., Viola, M., Barbouri, D., Kletsas, D., Passi, A., and Karamanos, N.K. (2014). Dynamic interplay between breast cancer cells and normal endothelium mediates the expression of matrix macromolecules, proteasome activity and functional properties of endothelial cells. Biochim. Biophys. Acta *1840*, 2549–2559.

Hanahan, D., and Weinberg, R.A. (2011). Hallmarks of cancer: the next generation. Cell *144*, 646–674.

Hetz, C. (2009). The UPR as a survival factor of cancer cells: More than folding proteins? Leuk. Res. *33*, 880–882.

Hetz, C. (2012). The unfolded protein response: controlling cell fate decisions under ER stress and beyond. Nat. Rev. Mol. Cell Biol. *13*, 89–102.

Horlbeck, M.A., Xu, A., Wang, M., Bennett, N.K., Park, C.Y., Bogdanoff, D., Adamson, B., Chow, E.D., Kampmann, M., Peterson, T.R., et al. (2018). Mapping the Genetic Landscape of Human Cells. Cell *174*, 953–967.

Hotamisligil, G.S., and Davis, R.J. (2016). Cell Signaling and Stress Responses. Cold Spring Harb. Perspect. Biol. *8*, a006072.

Hull, R.L., Bogdani, M., Nagy, N., Johnson, P.Y., and Wight, T.N. (2015). Hyaluronan: A Mediator of Islet Dysfunction and Destruction in Diabetes? J. Histochem. Cytochem. *63*, 592–603.

Joy, R.A., Vikkath, N., and Ariyannur, P.S. (2018). Metabolism and mechanisms of action of hyaluronan in human biology. Drug Metab. Pers. Ther. *33*, 15–32.

Kaneiwa, T., Yamada, S., Mizumoto, S., Montaño, A.M., Mitani, S., and Sugahara, K. (2008). Identification of a novel chondroitin hydrolase in Caenorhabditis elegans. J. Biol. Chem. *283*, 14971–14979.

Kim, E.K., and Choi, E.-J. (2010). Pathological roles of MAPK signaling pathways in human diseases. Biochim. Biophys. Acta *1802*, 396–405.

Kuleshov, M.V., Jones, M.R., Rouillard, A.D., Fernandez, N.F., Duan, Q., Wang, Z., Koplev, S., Jenkins, S.L., Jagodnik, K.M., Lachmann, A., et al. (2016). Enrichr: a comprehensive gene set enrichment analysis web server 2016 update. Nucleic Acids Res. *44*, W90–W97.

Kurz, C.L., and Tan, M.-W. (2004). Regulation of aging and innate immunity in C. elegans. Aging Cell *3*, 185–193.

Laurent, T.C., Laurent, U.B., and Fraser, J.R. (1996). The structure and function of hyaluronan: An overview. Immunol. Cell Biol. *74*, A1–A7.

Li, H., Handsaker, B., Wysoker, A., Fennell, T., Ruan, J., Homer, N., Marth, G., Abecasis, G., and Durbin, R.; 1000 Genome Project Data Processing Subgroup (2009). The Sequence Alignment/Map format and SAMtools. Bioinformatics *25*, 2078–2079.

Majors, A.K., Austin, R.C., de la Motte, C.A., Pyeritz, R.E., Hascall, V.C., Kessler, S.P., Sen, G., and Strong, S.A. (2003). Endoplasmic reticulum stress induces hyaluronan deposition and leukocyte adhesion. J. Biol. Chem. *278*, 47223–47231.

Misra, S., Hascall, V.C., Markwald, R.R., and Ghatak, S. (2015). Interactions between Hyaluronan and Its Receptors (CD44, RHAMM) Regulate the Activities of Inflammation and Cancer. Front. Immunol. *6*, 201.

Morawski, M., Filippov, M., Tzinia, A., Tsilibary, E., and Vargova, L. (2014). ECM in brain aging and dementia. Prog. Brain Res. *214*, 207–227.

Nagy, N., Kaber, G., Johnson, P.Y., Gebe, J.A., Preisinger, A., Falk, B.A., Sunkari, V.G., Gooden, M.D., Vernon, R.B., Bogdani, M., et al. (2015a). Inhibition of hyaluronan synthesis restores immune tolerance during autoimmune insulitis. J. Clin. Invest. *125*, 3928–3940.

Nagy, N., Kuipers, H.F., Frymoyer, A.R., Ishak, H.D., Bollyky, J.B., Wight, T.N., and Bollyky, P.L. (2015b). 4-methylumbelliferone treatment and hyaluronan

Cell

inhibition as a therapeutic strategy in inflammation, autoimmunity, and cancer. Front. Immunol. *6*, 123.

Papy-Garcia, D., Christophe, M., Huynh, M.B., Fernando, S., Ludmilla, S., Sepulveda-Diaz, J.E., and Raisman-Vozari, R. (2011). Glycosaminoglycans, protein aggregation and neurodegeneration. Curr. Protein Pept. Sci. *12*, 258–268.

Patro, R., Duggal, G., Love, M.I., Irizarry, R.A., and Kingsford, C. (2017). Salmon provides fast and bias-aware quantification of transcript expression. Nat. Methods *14*, 417–419.

Reiling, J.H., Clish, C.B., Carette, J.E., Varadarajan, M., Brummelkamp, T.R., and Sabatini, D.M. (2011). A haploid genetic screen identifies the major facilitator domain containing 2A (MFSD2A) transporter as a key mediator in the response to tunicamycin. PNAS *108(29)*, 11756–11765.

Robert, L., and Labat-Robert, J. (2015). Longevity and aging: role of genes and of the extracellular matrix. Biogerontology *16*, 125–129.

Robertson, C. (2016). The extracellular matrix in breast cancer predicts prognosis through composition, splicing, and crosslinking. Exp. Cell Res. *343*, 73–81.

Ron, D., and Walter, P. (2007). Signal integration in the endoplasmic reticulum unfolded protein response. Nat. Rev. Mol. Cell Biol. *8*, 519–529.

Salmon, A.B., Sadighi Akha, A.A., Buffenstein, R., and Miller, R.A. (2008). Fibroblasts from naked mole-rats are resistant to multiple forms of cell injury, but sensitive to peroxide, ultraviolet light, and endoplasmic reticulum stress. J. Gerontol. A Biol. Sci. Med. Sci. *63*, 232–241.

Sano, R., and Reed, J.C. (2013). ER stress-induced cell death mechanisms. Biochim. Biophys. Acta *1833*, 3460–3470.

Shalem, O., Sanjana, N.E., Hartenian, E., Shi, X., Scott, D.A., Mikkelson, T., Heckl, D., Ebert, B.L., Root, D.E., Doench, J.G., and Zhang, F. (2014). Genome-scale CRISPR-Cas9 knockout screening in human cells. Science *343*, 84–87.

Sherman, L.S., Matsumoto, S., Su, W., Srivastava, T., and Back, S.A. (2015). Hyaluronan Synthesis, Catabolism, and Signaling in Neurodegenerative Diseases. Int. J. Cell Biol. Published online September 10, 2015. https://doi.org/10.1155/2015/368584.

Shivers, R.P., Kooistra, T., Chu, S.W., Pagano, D.J., and Kim, D.H. (2009). Tissue-specific activities of an immune signaling module regulate physiological responses to pathogenic and nutritional bacteria in C. elegans. Cell Host Microbe *6*, 321–330.

Singh, V., and Aballay, A. (2006). Heat-shock transcription factor (HSF)-1 pathway required for Caenorhabditis elegans immunity. Proc. Natl. Acad. Sci. USA *103*, 13092–13097.

Sui, X., Kong, N., Ye, L., Han, W., Zhou, J., Zhang, Q., He, C., and Pan, H. (2014). p38 and JNK MAPK pathways control the balance of apoptosis and autophagy in response to chemotherapeutic agents. Cancer Lett. *344*, 174–179.

Taylor, R.C., and Dillin, A. (2013). XBP-1 is a cell-nonautonomous regulator of stress resistance and longevity. Cell *153*, 1435–1447.

Taylor, R.C., Berendzen, K.M., and Dillin, A. (2014). Systemic stress signalling: understanding the cell non-autonomous control of proteostasis. Nat. Rev. Mol. Cell Biol. *15*, 211–217.

Tian, X., Azpurua, J., Hine, C., Vaidya, A., Myakishev-Rempel, M., Ablaeva, J., Mao, Z., Nevo, E., Gorbunova, V., and Seluanov, A. (2013). High-molecular-mass hyaluronan mediates the cancer resistance of the naked mole rat. Nature *499*, 346–349.

Tigges, J., Krutmann, J., Fritsche, E., Haendeler, J., Schaal, H., Fischer, J.W., Kalfalah, F., Reinke, H., Reifenberger, G., Stühler, K., et al. (2014). The hallmarks of fibroblast ageing. Mech. Ageing Dev. *138*, 26–44.

Tolg, C., McCarthy, J.B., Yazdani, A., and Turley, E.A. (2014). Hyaluronan and RHAMM in wound repair and the "cancerization" of stromal tissues. BioMed Res. Int. Published online August 24, 2014. https://doi.org/10.1155/2014/103923.

Vigetti, D., Viola, M., Karousou, E., Rizzi, M., Moretto, P., Genasetti, A., Clerici, M., Hascall, V.C., De Luca, G., and Passi, A. (2008). Hyaluronan-CD44-ERK1/2 regulate human aortic smooth muscle cell motility during aging. J. Biol. Chem. *283*, 4448–4458.

Vigetti, D., Karousou, E., Viola, M., Deleonibus, S., De Luca, G., and Passi, A. (2014). Hyaluronan: biosynthesis and signaling. Biochim. Biophys. Acta *1840*, 2452–2459.

Walter, P., and Ron, D. (2011). The unfolded protein response: from stress pathway to homeostatic regulation. Science *334*, 1081–1086.

Wang, S., and Kaufman, R.J. (2012). The impact of the unfolded protein response on human disease. J. Cell Biol. *197*, 857–867.

Wang, T., Wei, J.J., Sabatini, D.M., and Lander, E.S. (2014). Genetic screens in human cells using the CRISPR-Cas9 system. Science *343*, 80–84.

Wang, W., Wang, J., and Li, F. (2017). Hyaluronidase and Chondroitinase. Adv. Exp. Med. Biol. *925*, 75–87.

Williams, K.W., Liu, T., Kong, X., Fukuda, M., Deng, Y., Berglund, E.D., Deng, Z., Gao, Y., Liu, T., Sohn, J.W., et al. (2014). Xbp1s in Pomc neurons connects ER stress with energy balance and glucose homeostasis. Cell Metab. *20*, 471–482.

Wu, J., and Kaufman, R.J. (2006). From acute ER stress to physiological roles of the Unfolded Protein Response. Cell Death Differ. *13*, 374–384.

Xu, C., Bailly-Maitre, B., and Reed, J.C. (2005). Endoplasmic reticulum stress: cell life and death decisions. J. Clin. Invest. *115*, 2656–2664.

Yamada, S., Sugahara, K., and Ozbek, S. (2011). Evolution of glycosaminoglycans: Comparative biochemical study. Commun. Integr. Biol. *4*, 150–158.

Yamamoto, H., Tobisawa, Y., Inubushi, T., Irie, F., Ohyama, C., and Yamaguchi, Y. (2017). A mammalian homolog of the zebrafish transmembrane protein 2 (TMEM2) is the long-sought-after cell-surface hyaluronidase. J. Biol. Chem. *292*, 7304–7313.

Youngman, M.J., Rogers, Z.N., and Kim, D.H. (2011). A decline in p38 MAPK signaling underlies immunosenescence in Caenorhabditis elegans. PLoS Genet. *7*, e1002082.

Zhao, Y., Gilliat, A.F., Ziehm, M., Turmaine, M., Wang, H., Ezcurra, M., Yang, C., Phillips, G., McBay, D., Zhang, W.B., et al. (2017). Two forms of death in ageing Caenorhabditis elegans. Nat. Commun. *8*, 15458.

Cell

STAR★METHODS

KEY RESOURCES TABLE

REAGENT or RESOURCE	SOURCE	IDENTIFIER
BACTERIAL AND VIRUS STRAINS		
OP50	CGC	N/A
HT115	CGC	N/A
PA14	CGC	N/A
DH5α	Invitrogen	18258012
Stbl3	Thermo Fisher	C7373-03
CHEMICALS, PEPTIDES, AND RECOMBINANT PROTEINS		
4μ8C	EMD Millipore	412512
(+)-5-Fluorodeoxyuridine (FUDR)	Spectrum Chemical	50-91-9
A-(2→3.6.8.9) Neuraminidase	Sigma-Aldrich	N8271
AEG 3482	TOCRIS	2651
Agarose, low melting	Sigma-Aldrich	A9414-10G
Ammonium Acetate	Sigma-Aldrich	A1542
Bacto Peptone	Fisher Scientific	DF0118072
BD Difco granulated agar	VWR	90000-782
Blasticidin S HCL	Thermo Fisher	A11139-03
BODIPY 493/503	Thermo Fisher	D3922
Calcium chloride dehydrate	VWR	97061-904
Carbenicillin	BioPioneer	C0051-25
Cholesterol	Sigma-Aldrich	57-88-5
Cytochalasin D	Cayman Chemical	11330
DEL 22379	TOCRIS	5774
DMEM media	Thermo Fisher	11995-073
DNase I	New England Biolabs	M03035
DTT	Sigma Aldrich	C2920
FBS, Premium Grade 500 ml (Lot# 190B14)	VWR	97068-091
FCCP	Cayman Chemical	CAS 370-86-5
Gentamicin	VWR	17-5182
GlutaMAX supplement	Thermo Fisher	35050-061
GSK2606414	Cayman Chemical	17376
Herculase II Fusion DNA Polymerase	Agilent	600677
Hyaluronan, various sizes	R&D Systems	GLR001
Hyaluronidase, sheep	Abcam	ab208484
IPTG dioxane free	Denville Scientific	CI8280-4
Lipofectamine 2000	Thermo Fisher	1-3603
LB Broth Miller	Fisher Scientific	BP1426500
LPS (O55:B5)	Sigma Aldrich	L2880
Magnesium sulfate heptahydrate	VWR	EM-MX0070-3
Non-essential Amino Acids solution	Thermo Fisher	11140-050
Opti-MEM	Thermo Fisher	4916
PBS, pH 7.4	Thermo Fisher	10010-049
Penicillin/Streptomycin solution	Thermo Fisher	15070-063
Polybrene	Fisher Scientific	TR-1003-G
Potassium Chloride	Fisher	P217-500

(Continued on next page)

Cell

Continued

REAGENT or RESOURCE	SOURCE	IDENTIFIER
Potassium phosphate dibasic	VWR	EM-PX1570-2
Potassium phosphate monobasic	VWR	EM-PX1565-5
Proteinase K	QIAGEN	19131
Puromycin dihydrochloride	Thermo Fisher	A11138-03
RNase A	QIAGEN	19101
Rifampicin	Fisher	BP2679250
Salubrinal	Chem Scene	CS-1012
SB 202190	Sigma Aldrich	S7067
SB 239062	TOCRIS	1962
SCH772984	Selleck Chemicals	S7101
Sodium Arsenite	Santa Cruz Biotechnology	Sc-301816
Sodium Azide	Sigma-Aldrich	71289-50G
Sodium Chloride	EMD Millipore	SX0420-5
Sodium phosphate dibasic	VWR	71003-472
Sodium phosphate monobasic monohydrate	Sigma-Aldrich	S9638-1KG
SP600125	Sigma-Aldrich	S5567
STF-083010	Cayman Chemical	17370
SU 5413	Cayman Chemical	13342
TE buffer	Sigma-Aldrich	T9285
Tetracycline hydrochloride	Sigma-Aldrich	T7660-5G
Trypsin-EDTA	Thermo Fisher	25200-072
Tunicamycin	Sigma-Aldrich	T7765-50MG
VEGF Recombinant Human Protein	Thermo Fisher	PHC9394
CRITICAL COMMERCIAL ASSAYS		
CellTiter-Glo Luminescent Cell Viability Assay	Promega	G7571
HA ELISA kit:: Human Hyaluronic Acid	MyBioSource	MBS262948
Pierce Detergent Compatible Bradford Assay Kit	Fisher Scientific	23246
QIAquick Gel Extraction Kit	QIAGEN	28706
QIAquick PCR Purification Kit	QIAGEN	28106
QIAGEN RNeasy Mini Kit	QIAGEN	74106
QIAprep Spin Miniprep Kit	QIAGEN	27106
DEPOSITED DATA		
C. elegans RNaseq	Mendeley	https://data.mendeley.com/datasets/dy97pwyf74/1
Human RNaseq & Screen Data	N/A	https://doi.org/10.17632/tmtkc8gcs8.1
EXPERIMENTAL MODELS: CELL LINES		
HEK293T	ATCC	CRL-11268
Human foreskin fibroblast, BJ	ATCC	CRL-2522
Human BJ fibroblast, pLentiCas9-Blast; pSGR119puro TMEM2.1 polyclonal	This study	N/A
Human BJ fibroblast, pLentiCas9-Blast; pSGR120puro TMEM2.2 polyclonal	This study	N/A
Human BJ fibroblast, pLentiCas9-Blast; pSGR121puro TMEM2.3 polyclonal	This study	N/A
Human BJ fibroblast, TMEM2-KO clonal: pLentiCas9-Blast; pSGR121puro clonal expansion	This study	N/A
Human BJ fibroblast, TMEM2-KO clonal + sSGRscramble.1gent	This study	N/A

(Continued on next page)

Cell

Continued

REAGENT or RESOURCE	SOURCE	IDENTIFIER
Human BJ fibroblast, TMEM2-KO clonal + sSGRscramble.2gent	This study	N/A
Human BJ fibroblast, TMEM2-KO clonal + sSGRscramble.3gent	This study	N/A
Human BJ fibroblast, TMEM2-KO clonal + sSGR49 gent ERN1.1	This study	N/A
Human BJ fibroblast, TMEM2-KO clonal + sSGR50 gent ERN1.2	This study	N/A
Human BJ fibroblast, TMEM2-KO clonal + sSGR51 gent ERN1.3	This study	N/A
Human BJ fibroblast, TMEM2-KO clonal + sSGR52 gent EIF2AK3.1	This study	N/A
Human BJ fibroblast, TMEM2-KO clonal + sSGR53 gent EIF2AK3.2	This study	N/A
Human BJ fibroblast, TMEM2-KO clonal + sSGR54 gent EIF2AK3.3	This study	N/A
Human BJ fibroblast, TMEM2-KO clonal + sSGR58 gent ATF6.1	This study	N/A
Human BJ fibroblast, TMEM2-KO clonal + sSGR59 gent ATF6.2	This study	N/A
Human BJ fibroblast, TMEM2-KO clonal + sSGR60 gent ATF6.3	This study	N/A
Human BJ fibroblast, TMEM2-KO clonal + sSGR199 gent CD44.1	This study	N/A
Human BJ fibroblast, TMEM2-KO clonal + sSGR200 gent CD44.2	This study	N/A
Human BJ fibroblast, TMEM2-KO clonal + sSGR201 gent CD44.3	This study	N/A
Human BJ fibroblast, TMEM2-KO clonal + sSGR202 gent RHAMM.1	This study	N/A
Human BJ fibroblast, TMEM2-KO clonal + sSGR203 gent RHAMM.2	This study	N/A
Human BJ fibroblast, TMEM2-KO clonal + sSGR204 gent RHAMM.3	This study	N/A
Human BJ fibroblast, TMEM2-KO clonal + sSGR205 gent ICAM.1	This study	N/A
Human BJ fibroblast, TMEM2-KO clonal + sSGR206 gent ICAM.2	This study	N/A
Human BJ fibroblast, TMEM2-KO clonal + sSGR207 gent ICAM.3	This study	N/A
Human BJ fibroblast, TMEM2-KO clonal +CMV-TMEM2gent	This study	N/A
Human BJ fibroblast, TMEM2-KO clonal +CMV-TMEM2 ΔP265Cgent	This study	N/A
Human BJ fibroblast, TMEM2-KO clonal +CMV-TMEM2 ΔD273Ngent	This study	N/A
Human BJ fibroblast, TMEM2-KO clonal +CMV-TMEM2 ΔD275Ngent	This study	N/A
EXPERIMENTAL MODELS: ORGANISMS/STRAINS		
C. elegans: Bristol (N2) strain as wild type (WT)	CGC	N2
C. elegans: SJ4005: zcls4(hsp-4p::GFP)V	(Taylor and Dillin, 2013)	SJ4005
C. elegans: RE666: ire-1(v33)II	CGC	RE666
C. elegans: AU78: agls219 [T24B8.5p::GFP::unc-54-3′ UTR + ttx-3p:: GFP::unc-54-3′ UTR] III	CGC	AU78
*C. elegans:*AGD1049: xbp-1(zc12) III	(Taylor and Dillin, 2013)	N/A
*C. elegans:*AGD1952; N2, uthIs485(sur-5p::hTMEM2::unc-54 UTR, myo-2p::tdtomato) strain C4a	This study (Taylor and Dillin, 2013)	N/A
*C. elegans:*AGD1953; N2, UTHIS486(SUR-5P::HTMEM2::UNC-54 UTR, MYO-2P::TDTOMATO) STRAIN G4E	THIS STUDY	N/A
C. ELEGANS: AGD1940: UTHEX847(SUR-5P::TMEM2::UNC-54 UTR; MYO-2P::TDTOMATO); ZCIS4[HSP-4P::GFP]	This study	N/A
C. elegans: AGD1961; N2, uthEx852(rgef-1p::hTMEM::unc-54 UTR, myo-2p::tdtomato)	This study	N/A
C. elegans: AGD2004: N2, uthIs486(sur-5p::hTMEM::unc-54 UTR, myo-2p::tdtomato) strain G4e; xbp-1(zc12)III	This study	N/A
C. elegans: AGD2005: N2, uthIs486(sur-5p::hTMEM::unc-54 UTR, myo-2p::tdtomato) strain G4e; ire-1(v33)II	This study	N/A
C. elegans: AGD2121: N2, uthEx870(vha-6p::hTMEM2::unc-54 UTR; myo-2p::tdtomato)	This study	N/A
C. elegans: AGD2343: N2, uthIs486(sur-5p::hTMEM::unc-54 UTR, myo-2p::tdTomato) strain G4e; uthIs270[rab-3p::xbp-1 s, myo-2p:: tdTomato]	This study	N/A
C. elegans: AGD2357: N2, uthIs486(sur-5p::hTMEM::unc-54 UTR, myo-2p::tdTomato) strain G4e; zcls4[hsp-4p::GFP]V	This study	N/A

Cell

REAGENT or RESOURCE	SOURCE	IDENTIFIER
C. elegans: AGD2416: N2, agIs219 [T24B8.5p::GFP::unc-54-3′ UTR + ttx-3p::GFP::unc-54-3′ UTR] III; uthIs486(sur-5p::hTMEM::unc-54 UTR, myo-2p::tdt)	This study	N/A
C. elegans: AGD2484: N2, uthEx924(sur-5p::hTMEM2 (R265C, D273N, D286N)::unc-54 UTR, myo-2p::tdt)	This study	N/A
OLIGONUCLEOTIDES		
All oligos ordered from IDT	Table S3	N/A
RECOMBINANT DNA		
pCMV-TMEM2gent: pCDH-CMV-TMEM2-MCS-EF1a-Gentamicin	This study	N/A
pCMV-TMEM2ΔP265Cgent: pCDH-CMV-TMEM2ΔP265C-MCS-EF1a-Gentamicin	This study	N/A
pCMV-TMEM2ΔD273Ngent: pCDH-CMV-TMEM2ΔD273N-MCS-EF1a-Gentamicin	This study	N/A
pCMV-TMEM2ΔD275Ngent: pCDH-CMV-TMEM2ΔD275N-MCS-EF1a-Gentamicin	This study	N/A
pEK2: myo-2p::tdtomato::unc-54 3′ UTR	This study	N/A
pFUDW LentiCas9-Blast	Addgene	52962
pRHS47: sur-5p::hTMEM2::unc-54 3′ UTR	This study	N/A
pRHS48: rgef-1p::hTMEM2::unc-54 3′ UTR	This study	N/A
pRHS49: vha-6p::hTMEM2::unc-54 3′ UTR	This study	N/A
pRHS54 sur-5p::hTMEM2(R265C, D273N, D286N)::unc-54 3′ UTR	This study	N/A
pSGRscramble.1puro; pHKO_42-pLKO-(N)_10-U6-sgScramble.1-EF1a-Puro	This study	N/A
pSGRscramble.1gent; pPF12-pLKO-(N)_10-U6-sgScramble.1-EF1a-Gentamycin	This study	N/A
pSGRscramble.2puro; pHKO_42-pLKO-(N)_10-U6-sgScramble.2-EF1a-Puro	This study	N/A
pSGRscramble.2gent; pPF12-pLKO-(N)_10-U6-sgScramble.2-EF1a-Gentamycin	This study	N/A
pSGRscramble.3puro; pHKO_42-pLKO-(N)_10-U6-sgScramble.3-EF1a-Puro	This study	N/A
pSGRscramble.3gent; pPF12-pLKO-(N)_10-U6-sgScramble.1-EF1a-Gentamycin	This study	N/A
pSGR49puro; pHKO_42-pLKO-(N)_10-U6-sgERN1.1-EF1a-Puro	This study	N/A
pSGR49 gent; pPF12-pLKO-(N)_10-U6-sgERN1.1-EF1a-Gentamycin	This study	N/A
pSGR50puro; pHKO_42-pLKO-(N)_10-U6-sgERN1.2-EF1a-Puro	This study	N/A
pSGR50 gent; pPF12-pLKO-(N)_10-U6-sgERN1.2-EF1a-Gentamycin	This study	N/A
pSGR51puro; pHKO_42-pLKO-(N)_10-U6-sgERN1.3-EF1a-Puro	This study	N/A
pSGR51 gent; pPF12-pLKO-(N)_10-U6-sgERN1.3-EF1a-Gentamycin	This study	N/A
pSGR52puro; pHKO_42-pLKO-(N)_10-U6-sgEIF2AK3.1-EF1a-Puro	This study	N/A
pSGR52 gent; pPF12-pLKO-(N)_10-U6-sgEIF2AK3.1-EF1a-Gentamycin	This study	N/A
pSGR53puro; pHKO_42-pLKO-(N)_10-U6-sgEIF2AK3.2-EF1a-Puro	This study	N/A
pSGR53 gent; pPF12-pLKO-(N)_10-U6-sgEIF2AK3.2-EF1a-Gentamycin	This study	N/A
pSGR54puro; pHKO_42-pLKO-(N)_10-U6-sgEIF2AK3.3-EF1a-Puro	This study	N/A
pSGR54 gent; pPF12-pLKO-(N)_10-U6-sgEIF2AK3.3-EF1a-Gentamycin	This study	N/A
pSGR58puro; pHKO_42-pLKO-(N)_10-U6-sgATF6.1-EF1a-Puro	This study	N/A
pSGR58 gent; pPF12-pLKO-(N)_10-U6-sgATF6.1-EF1a-Gentamycin	This study	N/A
pSGR59puro; pHKO_42-pLKO-(N)_10-U6-sgATF6.2-EF1a-Puro	This study	N/A
pSGR59 gent; pPF12-pLKO-(N)_10-U6-sgATF6.2-EF1a-Gentamycin	This study	N/A
pSGR60puro; pHKO_42-pLKO-(N)_10-U6-sgATF6.3-EF1a-Puro	This study	N/A

(Continued on next page)

Cell

Continued

REAGENT or RESOURCE	SOURCE	IDENTIFIER
pSGR119 gent; pPF12-pLKO-(N)_10-U6-sgTMEM2.1-EF1a-Gentamycin	This study	N/A
pSGR119puro; pHKO_42-pLKO-(N)_10-U6-sgTMEM2.1-EF1a-Puro	This study	N/A
pSGR120 gent; pPF12-pLKO-(N)_10-U6-sgTMEM2.2-EF1a-Gentamycin	This study	N/A
pSGR120puro; pHKO_42-pLKO-(N)_10-U6-sgTMEM2.2-EF1a-Puro	This study	N/A
pSGR121 gent; pPF12-pLKO-(N)_10-U6-sgTMEM2.3-EF1a-Gentamycin	This study	N/A
pSGR121puro; pHKO_42-pLKO-(N)_10-U6-sgTMEM2.3-EF1a-Puro	This study	N/A
pSGR60 gent; pPF12-pLKO-(N)_10-U6-sgATF6.3-EF1a-Gentamycin	This study	N/A
pSGR199puro; pHKO_42-pLKO-(N)_10-U6-sgCD44.1-EF1a-Puro	This study	N/A
pSGR199 gent; pPF12-pLKO-(N)_10-U6-sgCD44.1-EF1a-Gentamycin	This study	N/A
pSGR199puro; pHKO_42-pLKO-(N)_10-U6-sgCD44.1-EF1a-Puro	This study	N/A
pSGR199 gent; pPF12-pLKO-(N)_10-U6-sgCD44.1-EF1a-Gentamycin	This study	N/A
pSGR200puro; pHKO_42-pLKO-(N)_10-U6-sgCD44.2-EF1a-Puro	This study	N/A
pSGR200 gent; pPF12-pLKO-(N)_10-U6-sgCD44.2-EF1a-Gentamycin	This study	N/A
pSGR201puro; pHKO_42-pLKO-(N)_10-U6-sgCD44.3-EF1a-Puro	This study	N/A
pSGR201 gent; pPF12-pLKO-(N)_10-U6-sgCD44.3-EF1a-Gentamycin	This study	N/A
pSGR202puro; pHKO_42-pLKO-(N)_10-U6-sgRHAMM.1-EF1a-Puro	This study	N/A
pSGR202 gent; pPF12-pLKO-(N)_10-U6-sgRHAMM.1-EF1a-Gentamycin	This study	N/A
pSGR203puro; pHKO_42-pLKO-(N)_10-U6-sgRHAMM.2-EF1a-Puro	This study	N/A
pSGR203 gent; pPF12-pLKO-(N)_10-U6-sgRHAMM.2-EF1a-Gentamycin	This study	N/A
pSGR204puro; pHKO_42-pLKO-(N)_10-U6-sgRHAMM.3-EF1a-Puro	This study	N/A
pSGR204 gent; pPF12-pLKO-(N)_10-U6-sgRHAMM.3-EF1a-Gentamycin	This study	N/A
pSGR205puro; pHKO_42-pLKO-(N)_10-U6-sgICAM-1.1-EF1a-Puro	This study	N/A
pSGR205 gent; pPF12-pLKO-(N)_10-U6-sgICAM-1.1-EF1a-Gentamycin	This study	N/A
pSGR206puro; pHKO_42-pLKO-(N)_10-U6-sgICAM-1.2-EF1a-Puro	This study	N/A
pSGR206 gent; pPF12-pLKO-(N)_10-U6-sgICAM-1.2-EF1a-Gentamycin	This study	N/A
pSGR207puro; pHKO_42-pLKO-(N)_10-U6-sgICAM-1.3-EF1a-Puro	This study	N/A
pSGR207 gent; pPF12-pLKO-(N)_10-U6-sgICAM-1.3-EF1a-Gentamycin	This study	N/A
SOFTWARE AND ALGORITHMS		
ImageJ	NIH	N/A- download available from https://imagej.nih.gov/ij/
Prism7	GraphPad	N/A
GOrilla		http://cbl-gorilla.cs.technion.ac.il/

LEAD CONTACT AND MATERIALS AVAILABILITY

All strains and cell lines used in this study are available by direct request to the lead contact. Raw sequencing data are available in the following formats: *C. elegans* RNA-seq raw data are available at https://data.mendeley.com/datasets/dy97pwyf74/1. All human RNA-seq and screening raw data are available at https://doi.org/10.17632/tmtkc8gcs8.1. Further information and requests for resources and reagents should be directed to and will be fulfilled by the lead contact, Dr. Andrew Dillin (dillin@berkeley.edu).

EXPERIMENTAL MODEL AND SUBJECT DETAILS

For *C. elegans* work, all strains used are derivatives of N2 from Canorhabdities Genetics Center and specific genotypes of all strains used in this study are available in Key Resources Table. All worms are hermaphrodites for all studies. Specific growth conditions are specific under each experimental method detailed below. General growth and maintenance is as follows:

Cell

C. elegans growth and maintenance

All *C. elegans* strains used are derivatives of N2 from Caenorhabditis Genetics Center (CGC) and are listed in Key Resources Table. All worms are grown on NGM agar plates fed OP50 *E. coli* bacteria at 15°C. For experimentation, worms are synchronized via bleaching using a standard bleach solution (1.8% sodium hypochlorite, 0.375M KOH) until all carcasses are degraded and only eggs remain. The eggs are then washed 4x with M9 solution (22mM KH_2PO_4 monobasic, 42.3mM Na_2HPO_4, 85.6mM NaCl, 1mM $MgSO_4$) and spun at 20°C in M9 solution until eggs hatch and L1 worms are arrested (~12-16hours). L1s are then plated onto NGM agar plates containing μM IPTG, 100μg/ml carbenicillin, and 10μg/ml tetracycline and kept at 20°C until the desired stage. All experimental worms are fed HT115 *E. coli* bacteria harboring either empty vector (EV – pL4440) plasmids or pL4440 plasmids expressing double-stranded RNA containing the sequence of the target gene. All RNAi vectors were isolated from the Vidal libraries and sequence-verified prior to use.

All transgenic worms were synthesized by injecting N2 worms with plasmids listed in Key Resources Table at 25μg/ml with co-injection marker pEK2 (*myo-2p::tdtomato*) at 2.5μg/ml and 100μg/ml of pD64 vehicle as filler DNA. Worms positive for *myo-2p::tdtomato* were selected for stable arrays. Integration of *sur5p::hTMEM2* worms was performed by gamma irradiation. L4 worms were irradiated with 4400 rems of radiation and integrants were identified by selectin animals that maintained 100% *myo-2p::tdtomato* at 100% frequency past the F3 generation. Three independent lines were isolated, backcrossed to N2 animals 8x to eliminate mutations, and animals with the most similar phenotypes to the array animals were used for the experiment.

Cell culture and maintenance of human fibroblasts

We used the human foreskin fibroblast line BJ ATCC® CRL-2522 (BJ fibroblasts). The cells were cultured at 37°C, 95% air and 5% CO_2 in a humidified incubator on gelatin-coated dishes in medium containing DMEM, 15% Fetal Bovine Serum (FBS), 1% Glutamax, 1% Non-Essential Amino Acids (NEAA) and 1% Penicillin/Streptomycin. When cells reached confluence, the cells were washed with PBS, trypsinized and replated in a 1:3 to 1:6 split ratio, or used for experimental purposes. Media was replaced every other day, if necessary cells were frozen in maintenance media +10% DMSO. Human fibroblast cells are expressing Cas9 and hTERT in all experiments performed and are labeled as Wild-type.

Cell counting

Cells were counted using Countess FL II automated cell counter (Thermo Fisher; AMQAF1000) in 4x replicates (n = 4) per cell line.

METHOD DETAILS

C. elegans induction of ER stress and immune response reporter

Animals were synchronized to the L4 stage and treated with 25μg/ml Tunicamycin in M9 buffer for 4 h spinning at 20°C. Control animals were treated with an equal concentration of DMSO vehicle in M9 buffer (1% for concentrations used in this study). After 4 h of incubation, animals were washed with M9 buffer 2x, then plated onto OP50 plates overnight (~16 h) at 20°C to recover and allow for *hsp-4p::GFP* expression. Animals were picked at random (under white light) from a population and immobilized in 100nM sodium azide and lined up with pharynx facing up on an NGM plate. Worms were imaged using a Leica M250FA automated fluorescent stereomicroscope equipped with a Hamamatsu ORCA-ER camera.

For aging experiments, age-synchronized animals were grown on EV RNAi from hatch at 20°C and manually moved away from progeny onto new RNAi plates, similar to lifespans. Worms were moved onto 1% DMSO or 25μg/ml Tunicamycin plates containing EV RNAi 16 h prior to imaging (L4 for D1 imaging, D3 for D4 imaging, etc.). Imaging was performed similar to above.

For the immune response reporter, transgenic animals carrying *T24B8.5p::GFP* were synchronized to the L4 stage and moved to either EV or *pmk-1* RNAi. Animals were grown to adulthood and laid progeny, and the L4s from the second generation on RNAi were imaged using the similar protocol above.

C. elegans lifespan measurements

Lifespan measurements were performed on solid NGM agar plates spotted with RNAi bacteria (HT115 *E. coli* strain with either EV pL4440 or RNAi vectors). Worms were synchronized by bleaching, L1 arrested, and grown to adulthood at 20°C. Adult worms were moved away from progeny daily onto new RNAi plates until progeny were no longer visible (~7-10 days). Animals were then scored every 1-2 days for death until all animals were scored. Animals with bagging, vulval explosion, or other age-unrelated deaths were censored and removed from statistics. For Tunicamycin lifespans, either 1% DMSO, 5μg/ml Tunicamycin, 10μg/ml Tunicamycin, or 25μg/ml Tunicamycin was included in the NGM agar plates, and animals were moved onto DMSO or Tunicamycin plates at D1. All animals were grown on DMSO plates until D1 to allow proper development of animals, since tunicamycin results in developmental defects. Prism5 software was used for statistical analysis and log-rank (Mantel-Cox) method was used to determine significance. All lifespans are performed with the experimenter blinded to the identity of strains throughout the entirety of the experiment.

For *Pseudomonas aeruginosa* (PA14) lifespans, worms were synchronized by bleaching, L1 arrested, and grown to L4 at 20°C on NGM agar plates spotted with RNAi bacteria (HT115 *E. coli* strain with EV pL4440). Worms were then transferred onto solid agar plates (0.3% NaCl w/v; 0.35% peptone w/v; 1.7% agar w/v; 1mM $CaCl_2$; 1mM $MgSO_4$; 5ng/ml cholesterol; 1mM KPO_4) seeded

Cell

with 10μl of PA14 culture spread evenly along the surface of the plates 24 h prior. Animals were then scored every 6 h for death until all animals were scored. Bagged animals were scored as dead, and only animals crawling off the plates were considered censored in this assay.

For FUDR lifespans, worms were synchronized and grown on EV bacteria similar to above. Worms were then transferred onto agar plates seeded with EV and spotted with 100μl of 10mg/ml FUDR. Lifespans were scored similar to standard lifespans.

To kill bacteria for dead bacteria assays, NGM agar plates were spotted with RNAi bacteria (HT115 *E. coli* strain with EV pL4440) and allowed to dry overnight. Spotted plates were then put into a UV cross-linker (CL-1000 Ultraviolet Crosslinker; 254nm; Energy x100 μ J/cm^2) for ten min, where both the spotted plate and lids were exposed to UV treatment face up. Treated plates were left at room temperature overnight prior to using. Lifespans were carried out on these plates similar to standard lifespans described above.

C. elegans RNA-seq and analysis

Animals were synchronized and grown to D2 on EV RNAi plates. ~2,000 animals were harvested using M9. M9 was subsequently aspirated, replaced with trizol, and worms were freeze/thawed 3x with lipid nitrogen/37°C water bath cycles. After the final thaw, chloroform was added at a 1:5 ratio of chloroform:trizol volume for aqueous separation of RNA, which was performed via centrifugation in heavy gel phase-lock tubes (VWR, 10847-802). The aqueous phase was mixed with isopropanol, then RNA purification was performed using a QIAGEN RNeas Mini Kit as per manufacturer's directions. Library preparation was performed using Kapa Biosystems mRNA Hyper Prep Kit. Sequencing was performed using Illumina HS4000, mode SR100 through the Vincent J. Coates Genomic Sequencing Core at University of California, Berkeley. Reads were aligned and quantified using Salmon (Patro et al., 2017), with WBcel235 as the worm reference genome. Fold changes were determined using R-package DESeq2. For analysis of UPR[ER] genes, the GO term ER-UPR was used (GO 0030968). Enrichment was calculated using Gene Ontology enrichment analysis and visualization tool(Eden et al., 2009, 2007). It should be noted that both *sur-5p::hTMEM2* animals and *rab-3p::xbp-1 s* animals have a significant increase in *aex-5* transcripts. This is because the *unc-54* 3′UTR used in these transgenes has a small part of the last exon of *aex-5*. This serves as a validation that our transgenes are highly expressed in these animals.

CellTiter-Glo® luminescence viability assay

We experienced significant variation in the cell number plated based on cell counting alone. We therefore generally seeded each cell line in two concentrations in order to control for any cell density effects that might be contributing to the stress phenotype. Furthermore, we generally focused on results that are relative to the no treatment control conditions of each cell line, in order to allow us a comparison between cell lines. Cells were seeded at 100k and 200k/plate on gelatin-coated 24/well (VWR; 29442-044) or 96well (Corning; 3904) plates. After 24h the compounds were added to the plated cells. After an additional 5days, the plates were washed 1x with PBS and CellTiter-Glo/media (1:3), was added to the wells, 100μl/96well, 250μl/24well with a multichannel pipette. After an incubation of 30min at 37°C, luminescence of the 96well was measured using Tecan M1000. In case of the 24well plates, 100μl of each well was removed and added to a 96well (Corning; 3904), using a multichannel pipette, for measurement, in order to avoid interference of the measurements through diffraction. Wells on the periphery of the plate were generally avoided, due to differences in oxygen exposure and evaporation during the culture of these cells. For the statistical analysis of these experiments, we utilized a one-way ANOVA test with a post hoc Bonferroni-Holm analysis. All results presented here passed the equal variance test and normal distribution was assumed.

Clonal expansion

Single human fibroblast cells are often troublesome to expand. We therefore started by plating Wild-type fibroblast at 25k/plate density on a gelatin-coated 48well plate in order to support the initial stages of clonal fibroblast expansion. The cell line chosen for clonal expansion, was then added at a 0.5cells/well density to the Wild-type fibroblasts. As soon as the cells reached confluency, the initial transduction selection marker was used once more, this time to remove the supporting wild-type cells. The surviving cells were then left for expansion until the well was confluent (roughly 6-8 weeks). Part of the cells were then send for sequence validation, the rest frozen down until the clonal nature and successful genome editing was verified.

Clonal expansion of TMEM2 and control lines

For our initial attempt to characterize the impact of TMEM2 on ER stress resistance, we exposed a population of cells to CRISPR/Cas9 and sgRNA targeting TMEM2. This approach generates a complex mutant pool within this population of cells, some of which possess heterozygotic or homozygotic ablation of the targeted gene product, while others maintain two functional copies of the gene due to neutral modification of the targeted locus. We observed significant changes to ER stress resistance, due to the disruption of TMEM2 expression, when compared to Wild-type and scramble control conditions under this experimental paradigm (data not shown).

From this complex mutant pools we generated clonal lines of TMEM2. During the derivation of these clonal lines, we also generated Wild-type and scramble sgRNA clonal control lines, in order to test if the presence of scramble sgRNA or the clonal nature impacted ER stress resistance itself. We did not observe any significant differences between the clonal lines, between the pooled and clonal control lines, or due to the expression of scramble sgRNA, on ER stress resistance. However, ablation of TMEM2, be it of one or both

alleles, significantly reduced ER stress resistance as described in the results section. While we continued to include these controls in our characterization of the TMEM2 phenotype, the additional controls show no significant differences to the Wild-type controls, and therefore do not provide additional insight or information. We therefore decided to exclude the clonal control results for clarity and ease of the presentation of the results.

CRISPR/CAS9-mediated gene disruption

In order to target a specific genomic locus, we cloned single guide sgRNA vectors using the AVANA sgRNA library sequences, into the LENTI-viral expression vector pLKO.1. We then proceeded to transduce the fibroblasts with lenti-virus at an MOI of 0.3–0.5 (usually between 50-100μl of virus/well). We then added maintenance media to a total of 800μl/well. One well without viral transduction was included to the setup in order to serve as a selection control. Cells were incubated overnight and washed 2x with PBS and normal fibroblast culture media added. After 48h, the cells were then exposed to either Puromycin, Blasticidine or Gentamicin based on the selection cassette used. The selection was removed as soon as all the cells in the non-transduction control were dead, roughly after 5-7days. The cells were then cultured and expanded for an additional 7-14days in order to maximize genome editing efficacy and to allow for target protein depletion. Finally, the cells were then frozen down or immediately used for experiments.

Genomic DNA extraction and screen library preparation

For gDNA extraction $3x10^7$ - $5x10^7$ frozen cell pellet in a 15ml conical tube, 6ml of NK Lysis Buffer (50 mM Tris, 50 mM EDTA, 1% SDS, pH 8) and 30 μL of 20mg/ml Proteinase K were added to the tissue/cell sample and incubated at 55°C overnight. The next day, 30 μL of 10mg/ml RNase A, diluted in NK Lysis Buffer to 10mg/ml and then stored at 4°C, was added to the lysed sample, which was then inverted 25 times and incubated at 37°C for 30min. Samples were cooled on ice before addition of 2ml of pre-chilled 7.5M ammonium acetate to precipitate proteins. Stock solutions of 7.5M ammonium acetate was made in sterile dH2O and kept at 4°C until use. After adding ammonium acetate, the samples were vortexed at high speed for 20 s and then centrifuged at $\geq$ 4,000 × g for 10min. After the spin, a tight pellet was visible in each tube and the supernatant was carefully decanted into a new 15ml conical tube. Then 6ml 100% isopropanol was added to the tube, inverted 50 times and centrifuged at $\geq$ 4,000 × g for 10min. Genomic DNA was visible as a small white pellet in each tube. The supernatant was discarded, 6ml of freshly prepared 70% ethanol was added to the tube and inverted 10times.he tube was then centrifuged at $\geq$ 4,000 × g for 1min. The supernatant was discarded by pouring; the tube was briefly spun, and remaining ethanol was removed using a P200 pipette. After air drying for 10-30min, the DNA changed appearance from a milky white pellet to slightly translucent. At this stage, 500 μL of 1xTE buffer was added, the tube was incubated at 65°C for 1h and at room temperature overnight to fully resuspend the DNA. The next day, the gDNA samples were vortexed briefly. The gDNA concentration was measured using a Nanodrop (Thermo Scientific).

To measure the distribution of the different library sgRNA within each screen arm we used Illumina Next Generation Sequencing applied to an amplicon generated from a single targeted PCR of the integrated sgRNA cassette (PMID: 24336571). Briefly, we use all the collected gDNA (1000x coverage) divided into 100μl PCR reactions with 5μg of DNA per reaction. We used Herculase Fusion II DNA polymerase using the default mix protocol only with double the amount of primers. PCR program: (950 2min, (980 10sec, 600 30sec, 720 30sec) x 24, 720 5min). As forward primer for all samples we used an equimolar mix of the following primers:

Illumina sequences	Stagger	Priming site
AATGATACGGCGACCACCGAGATCTACACTCTTTCCC TACACGACGCTCTTCCGATCT	t	Tcttgtggaaaggacgaaacaccg
AATGATACGGCGACCACCGAGATCTACACTCTTTCCC TACACGACGCTCTTCCGATCT	at	Tcttgtggaaaggacgaaacaccg
AATGATACGGCGACCACCGAGATCTACACTCTTTCCC TACACGACGCTCTTCCGATCT	gat	Tcttgtggaaaggacgaaacaccg
AATGATACGGCGACCACCGAGATCTACACTCTTTCCC TACACGACGCTCTTCCGATCT	cgat	Tcttgtggaaaggacgaaacaccg
AATGATACGGCGACCACCGAGATCTACACTCTTTCCC TACACGACGCTCTTCCGATCT	tcgat	Tcttgtggaaaggacgaaacaccg
AATGATACGGCGACCACCGAGATCTACACTCTTTCCC TACACGACGCTCTTCCGATCT	atcgat	Tcttgtggaaaggacgaaacaccg
AATGATACGGCGACCACCGAGATCTACACTCTTTCCC TACACGACGCTCTTCCGATCT	gatcgat	Tcttgtggaaaggacgaaacaccg

Cell

One of the following reverse primers was used to each sample

Illumina sequence	Sample specific barcode	Illumina sequence	Priming site
CAAGCAGAAGACGGC ATACGAGAT	AAGTAGAG	GTGACTGGAGTTCAGACG TGTGCTCTTCCGATCT	TCTACTATTCTTTCC CCTGCACTGT
CAAGCAGAAGACGGC ATACGAGAT	ACACGATC	GTGACTGGAGTTCAGACG TGTGCTCTTCCGATCT	TCTACTATTCTTTCC CCTGCACTGT
CAAGCAGAAGACGGC ATACGAGAT	CGCGCGGT	GTGACTGGAGTTCAGACG TGTGCTCTTCCGATCT	TCTACTATTCTTTCC CCTGCACTGT
CAAGCAGAAGACGGC ATACGAGAT	CATGATCG	GTGACTGGAGTTCAGACG TGTGCTCTTCCGATCT	TCTACTATTCTTTCC CCTGCACTGT
CAAGCAGAAGACGGC ATACGAGAT	CGTTACCA	GTGACTGGAGTTCAGACG TGTGCTCTTCCGATCT	TCTACTATTCTTTCC CCTGCACTGT

PCR products were gel purified and an equimolar mix was sequences of HiSeq2000 using standard Illumina primers.

Human Fibroblast RNaseq and analysis

RNA purification was performed using a QIAGEN RNase Mini Kit as per manufacturer's instructions. Library preparation was performed using Kapa Biosystems mRNA Hyper Prep Kit. Sequencing was performed using Illumina HS4000, mode SR100 through the Vincent J. Coates Genomic Sequencing Core at University of California, Berkeley. Trimmed fastq reads were then aligned to the human genome (GRCh38) using STAR RNaseq aligner (Dobin et al., 2013) version 2.5.2a using default parameters. Sam files were then converted to Bam files using Samtools (Li et al., 2009). Read counts per gene were calculated using the R bioconductor package GenomicAlignments with the function summarizeOverlaps with parameters: mode = "Union," singleEnd = TRUE, ignore.strand = TRUE. Differential expression fold change and significance where calculated using DEseq package (Anders and Huber, 2010).

Lentiviral production and transduction of expression vectors in general

HEK293T cells were seeded at ~40% confluence the day before transfection in D10 media on gelatin-coated 6well plates (VWR; 29442-042). One hour prior to transfection, media was removed and 1ml of pre-warmed reduced serum OptiMEM media was added to each well. We then mixed for each 6well, 2μg of the plasmid of choice, and the packaging vectors pMDLg/pRRE (1.3μg), pRSV.Rev (500ng) and pVSVg (700ng) to a total of 100μl OptiMEM. In a separate tube, we mixed 5μl/well Lipofectamine 2000 reagent diluted to 100μl with OptiMEM, and after 5min, added to the mixture of DNA/OptiMEM. The complete mixture was incubated for 20min before being added to the HEK293T cells. After 6h, the media was changed to 1ml/well fibroblast culture media. After 48h, the supernatant was collected and centrifuged at 3,000 rpm for 10min to pellet cell debris. The supernatant was then filtered through a 0.45μm low protein binding membrane (Millipore Steriflip HV/PVDF). Aliquots were stored at –80°C.

Library lentiviral production

Four 15cm² dishes (VWR; 430599) of HEK293T cells were seeded at ~40% confluency the day before transfection in D10 media (DMEM supplemented with 10% fetal bovine serum). One hour prior to transfection, media was removed and 13ml of pre-warmed reduced serum OptiMEM media was added to each dish. Transfection was performed using Lipofectamine 2000. For each dish, 20μg of plasmid library, 10μg of pVSVg, and 15μg of psPAX2 (Addgene) were diluted in 2ml OptiMEM (Life Technologies). 100μl of Lipofectamine 2000 was diluted in 2ml OptiMEM and, after 5min, it was added to the mixture of DNA. The complete mixture was incubated for 20min before being added to cells. After 6h, the media was changed to 15ml D10. Media containing lentiviral particles was removed after 48h and stored in 1ml aliquots at −80°C.

Screen cell culture

Human immortalized foreskin fibroblasts (BJ fibroblast) were cultured at 37°C, 95% air and 5% CO_2 in a humidified incubator on gelatin-coated dishes in medium containing DMEM, 15% Fetal Bovine Serum (FBS), 1% Glutamax, 1% Non-Essential Amino Acids (NEAA) and 1% Penicillin/Streptomycin in all experiments. Cells were transduced with the AVANA library via spinfection. To find optimal virus volumes for achieving an MOI of 0.3–0.5, each new virus lot was tested by spinfecting 2x10⁶ cells with several different volumes of virus. Briefly, 2x10⁶ cells per well were plated into a 12-well plate in media supplemented with 8μg/ml polybrene (Sigma). Each well received a different titrated virus amount (usually between 5 and 200μl) along with a no-transduction control. The 12-well plate was centrifuged at 1,000 g for 2h at 37°C and left in the incubator overnight. Media was aspirated the next morning and cells were enzymatically detached using trypsin. Cells were counted and each well was split into duplicate wells diluted 1:10. One replicate received 1μg/ml puromycin. After 3days cells were counted to calculate a percent transduction. Percent transduction is calculated as

cell count from the replicate with puromycin divided by cell count from the replicate without puromycin multiplied. The virus volume yielding a MOI closest to 0.4 was chosen for large-scale screening.

For the screen itself we aimed to maintain a 500x coverage over library complexity (80,000). We transduced 250×10^6 cells (divided into 12 well plates) using spinfection and the predetermined virus and cell amount. Day following transduction all cells were mixed together and plated on 60 15cm plated with puromycin selection. One well was used to ensure that the screen MOI was indeed as aimed using the same method described above. Cells were cultured for two weeks to maximize genome-editing and target protein depletion while maintaining a minimum of 40M cells (500x coverage) at all times. After two weeks cells were spitted to a control and treatment arm and cultured for an additional three weeks in the presence of 200ng/ml Tunicamycin or 0.1% DMSO, before harvesting gDNA.

Screening data analysis

To count the number of reads associated with each sgRNA in each fastq file, we first extracted the sgRNA targeting sequencing using a regular expression containing the three nucleotides flanking each side of the sgRNA 20bp target. sgRNA spacer sequences were then aligned to a pre-indexed AVANA library using the short-read aligner 'bowtie' using parameters –v 0 –m 1. Data analysis was performed using custom R scripts. Gene level p values were calculated using the mean of the four sgRNA compared to an empirical distribution of means generated by random data permutations.

QUANTIFICATION AND STATISTICAL ANALYSIS

All statistical analyses are specifically described in figure legends and in the experimental methods above. All graphical representations and sample sizes are also provided in the figure legends. PRISM software is used to perform all statistical tests.

DATA AND CODE AVAILABILITY

All necessary data to draw conclusions presented are available within the manuscript. Raw sequencing data are available in the following formats: *C. elegans* RNA-seq raw data are available at https://data.mendeley.com/datasets/dy97pwyf74/1 (Mendeley: https://doi.org/10.17632/dy97pwyf74.1). All human RNA-seq and screening raw data are available at https://doi.org/10.17632/tmtkc8gcs8.1 (https://doi.org/10.17632/tmtkc8gcs8.1). Further information and requests for resources and reagents should be directed to and will be fulfilled by the lead contact, Dr. Andrew Dillin (dillin@berkeley.edu). No program code has been used in this manuscript.
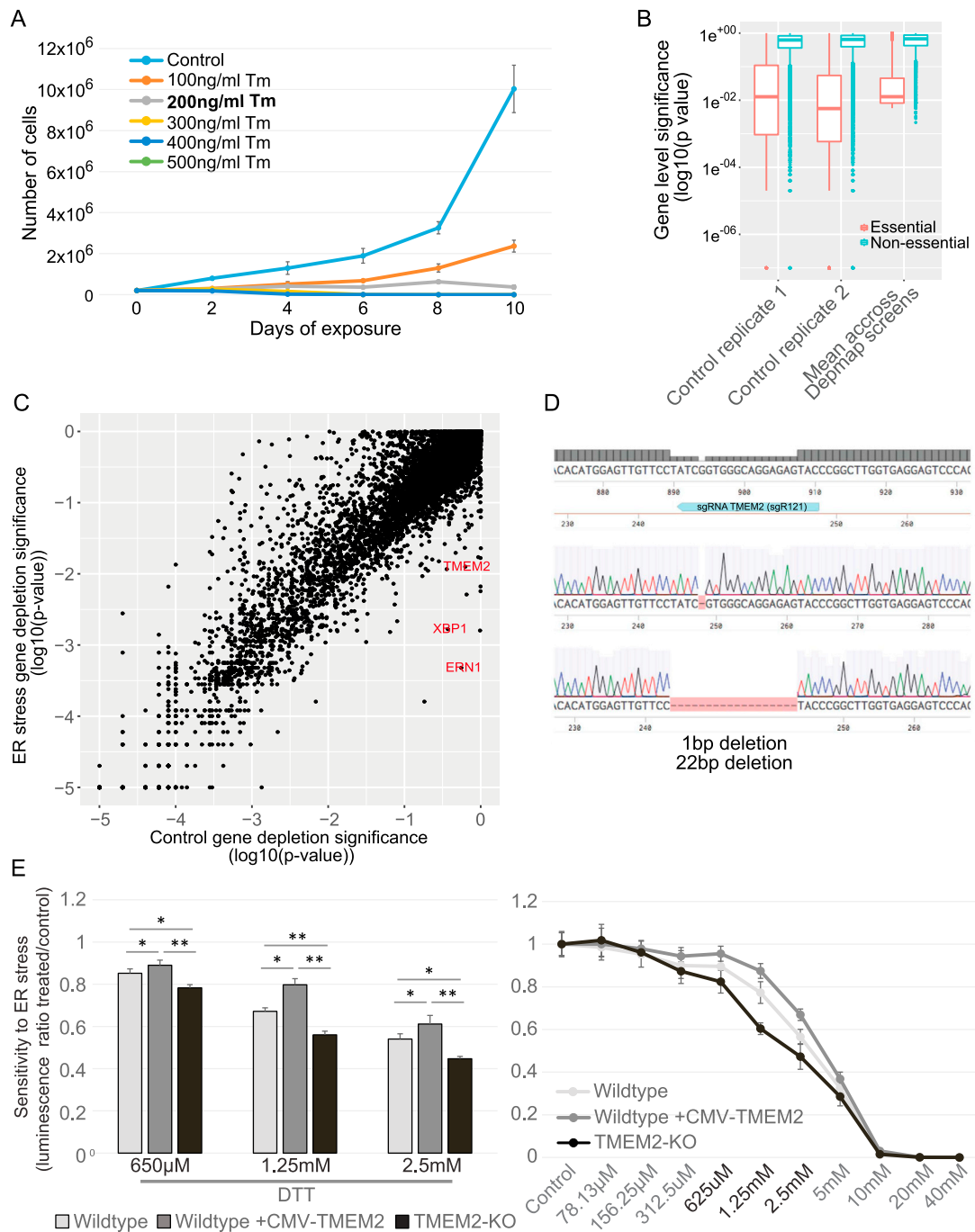
Figure S1. Related to Figure 1

A) Proliferation of human immortalized fibroblasts exposed to varying levels of Tunicamycin, as determined through cell counting (n = 3). 200ng/ml Tunicamycin was used for the whole genome KO screen. (**B**) Quantitative comparison of the depletion of essential genes in the control arm of the two screen replicates, compared to the mean depletion of > 400 screens that used the AVANA library (data downloaded from https://depmap.org/portal/). (**C**) Comparison of gene depletion p values (see STAR Methods) between Control and Tunicamycin-treated fibroblast in the second screen replicate. (**D**) Results of the sequence validation of the TMEM2 locus in TMEM2-KO clonal fibroblast line. (**E**) CellTiter-Glo (CTG) analysis to determine cell density of Wild-type, TMEM2-KO and CMV-TMEM2 overexpressing fibroblasts exposed to varying levels of DTT-induced ER stress, at the endpoint of a 5 day treatment. Results are presented relative to the untreated control conditions in order to adjust for cell number variability between the cell lines at the start of the experiment; (n = 3). Statistical Analysis: One-way ANOVA analysis with post hoc Bonferroni-Holm analysis; * = p < 0.05; ** = p < 0.01, *** = p < 0.001. All bar graphs represent mean. All error bars for all plots represent standard deviation.
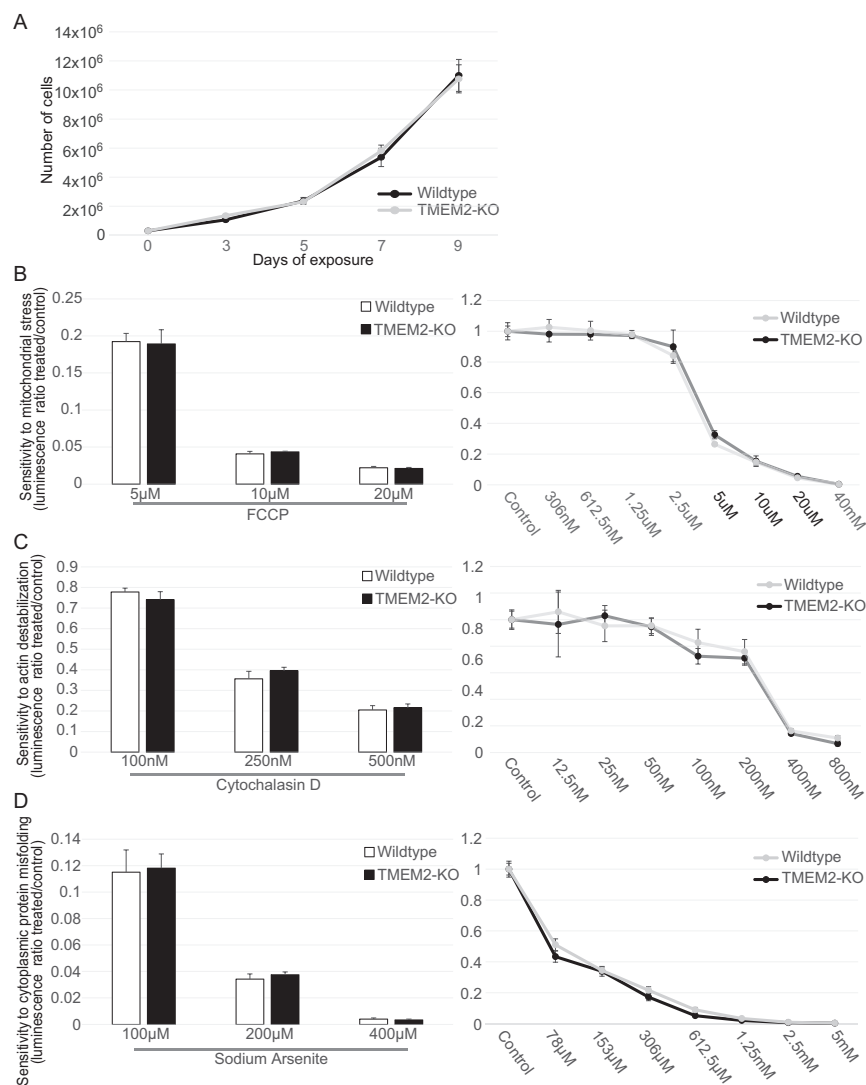
Figure S2. TMEM2-KO Fibroblast Showed No Changes in Proliferation or Resistance to Mitochondrial, Cytoplasmic Protein-Misfolding or Actin Destabilization Stress, Related to Figure 2

(**A**) Wild-type and TMEM2-KO fibroblast proliferation speed was determined through cell counting in the absence of cellular stress; (n = 3). (**B**) Resistance to FCCP-induced mitochondrial stress was measured in Wild-type and TMEM2-KO human fibroblasts. The cells were exposed to FCCP for 5 days and cell density measured at the endpoint of the experiment using CTG analysis; (n = 3). (**C**) Wild-type and TMEM2-KO cells were exposed to the actin destabilization compound Cytochalasin D for 5 days. Cell density was then determined via CTG analysis; (n = 3). (**D**) CTG analysis of TMEM2-KO to Wild-type fibroblast grown for 5 days in the presence and absence of Sodium Arsenite, a compound which induces cytoplasmic protein misfolding; (n = 3). All bar graphs represent mean. All error bars for all plots represent standard deviation.
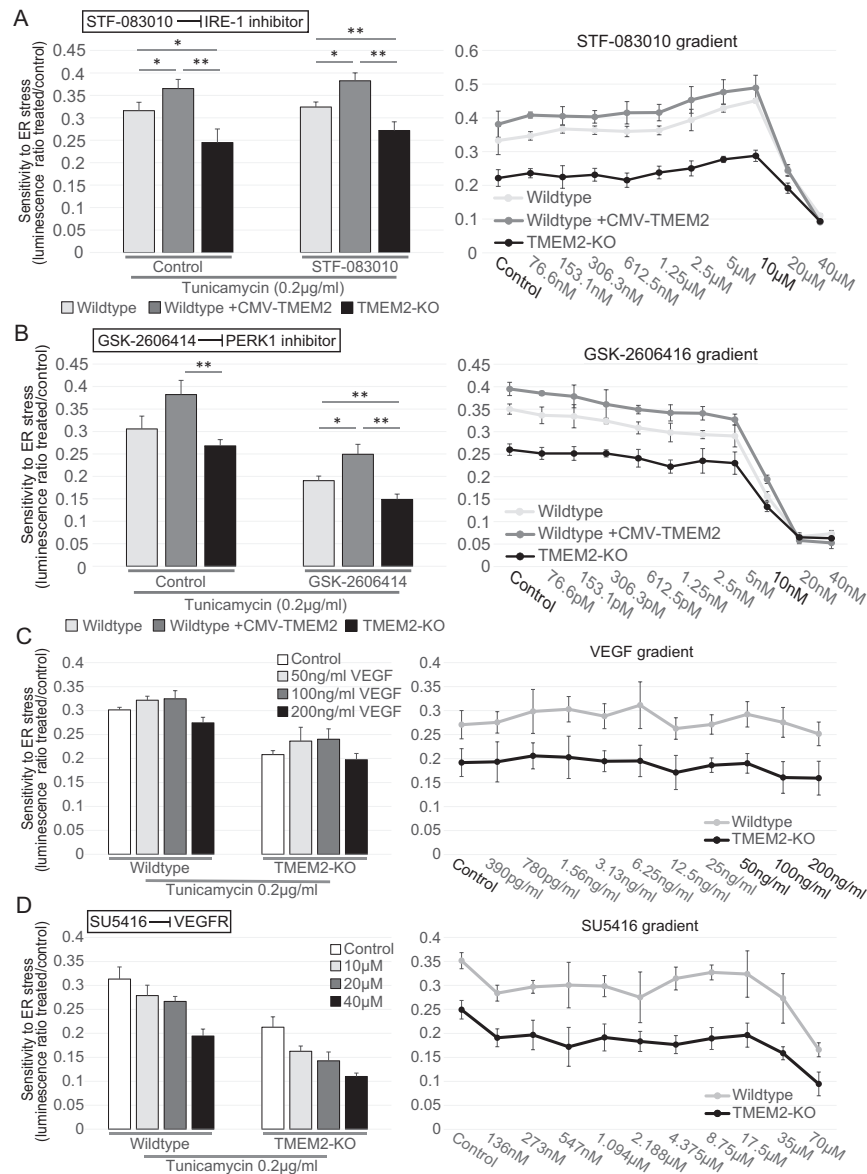
Figure S3. The Impact of TMEM2 on Stress Resistance Is Independent of the Canonical UPR[ER] Pathway Components IRE1 and PERK1, and It Does Not Involve VEGF Signaling, Related to Figures 3 and 4

A-B) Wild-type, TMEM2-KO and CMV-TMEM2 overexpressing human fibroblasts were exposed to varying concentrations of (**A**) the IRE-1-mediated XBP1-splicing inhibitor STF-083010 (Concentration in bar graphs: 10μM) (n = 3) or the (**B**) PERK1 inhibitor GSK-2606414 (Concentration in bar graphs: 10nM). Tunicamycin-induced ER stress resistance was monitored through CTG analysis after a 5 day treatment with 200ng/ml Tunicamycin; (n = 3). (**C**) CTG analysis of Wild-type and TMEM2-KO human fibroblasts was performed to determine the cell density after the exposure to Tunicamycin-induced ER-stress (5 days; 200ng/ml Tunicamycin), and in the presence or absence of the growth factor VEGF (n = 3). (**D**) CTG analysis of Wild-type, TMEM2-KO and CMV-TMEM2 overexpressing cells in the presence and absence of the VEGF receptor inhibitor SU5416 and Tunicamycin-induced ER stress (5 day exposure, Tunicamycin 200ng/ml) (n = 3). Statistical Analysis: One-way ANOVA analysis with post hoc Bonferroni-Holm analysis; * = p < 0.05; ** = p < 0.01, *** = p < 0.001. All bar graphs represent mean. All error bars for all plots represent standard deviation.
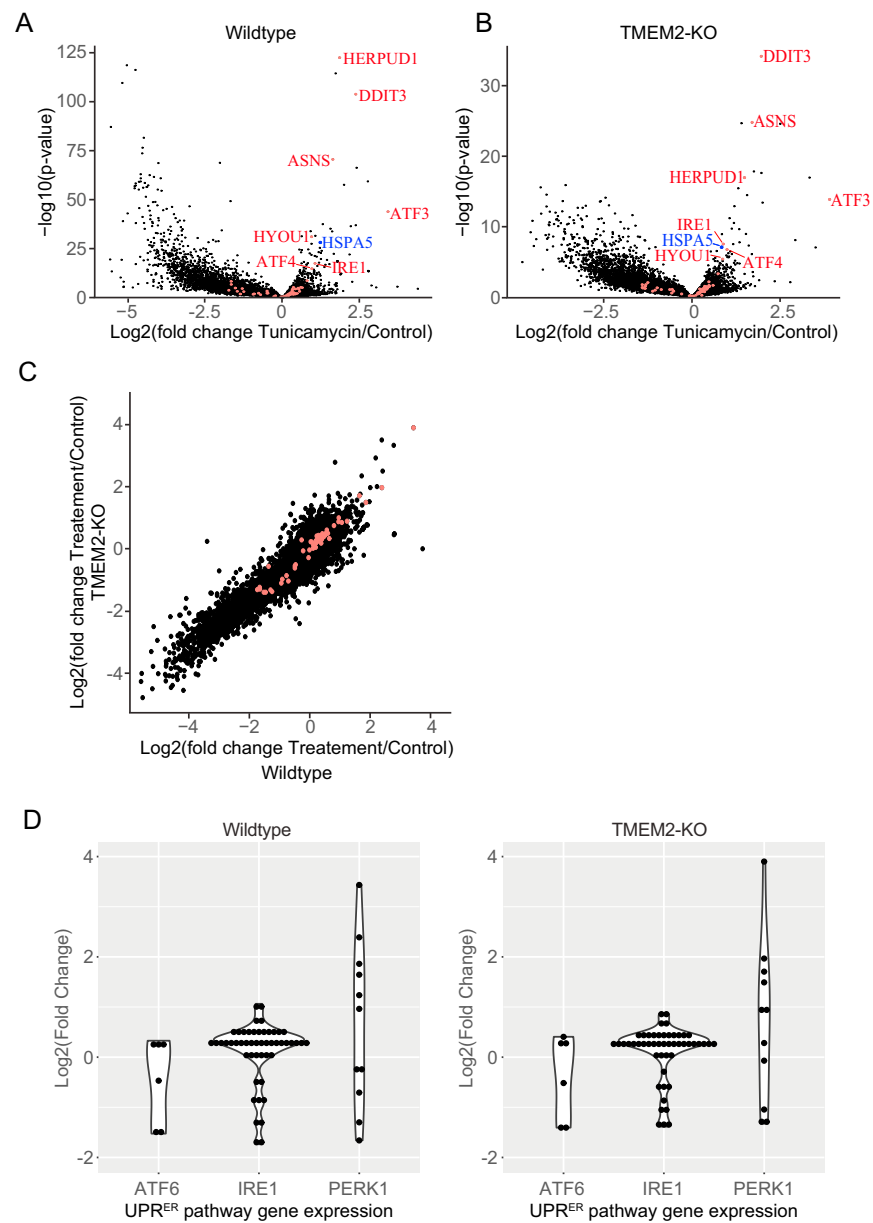
Figure S4. RNA-Seq Analysis of Wild-Type and TMEM2-KO Human Fibroblasts Reveals that TMEM2-KO Cells Are Capable of Inducing the UPR^ER in the Presence of ER Stress, Related to Figure 3

Volcano plot of (A) Wild-type and (B) TMEM2-KO cells, and their shift in gene expression in response to an 8h, 200ng/ml Tunicamycin treatment. Genes highlighted in red are known UPR^ER target genes, HSPA5 is highlighted in blue. (C) Dot plot comparing the response between the two cell lines, known UPR^ER target genes are highlighted in red; (D) Analysis of the expression changes in response to Tunicamycin treatment, of gene targets associated with each of the canonical UPR^ER pathways, ATF6, IRE1 and PERK1. Each point represents a gene mean expression across three replicate measurements (see STAR Methods for details of the analysis).
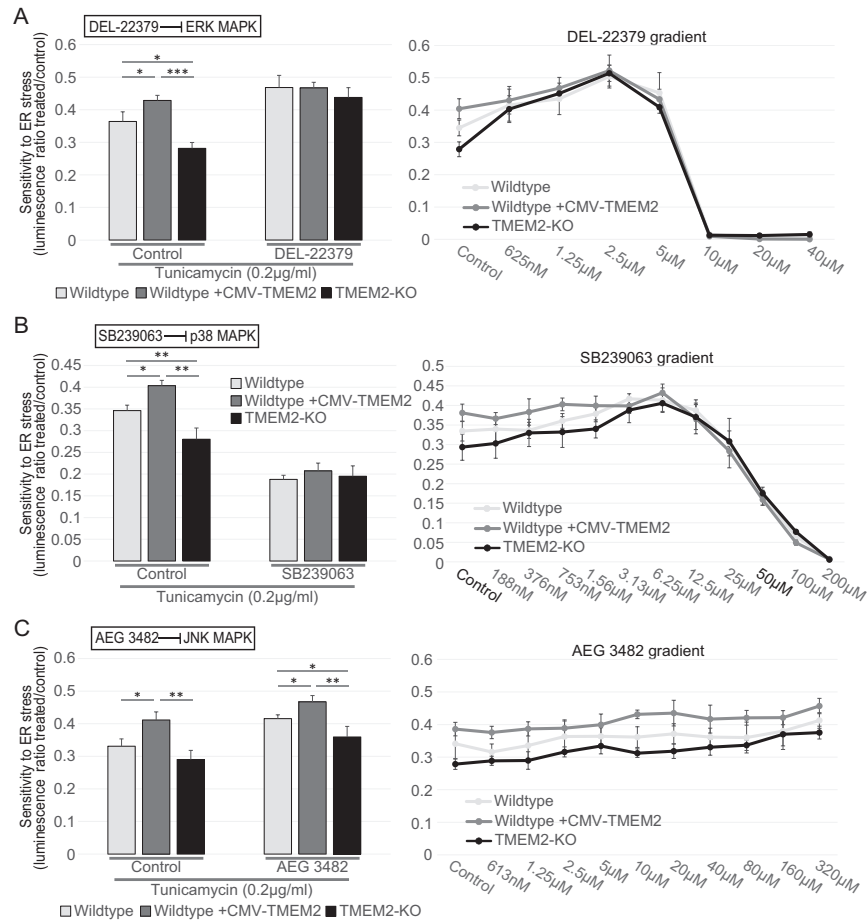
Figure S5. The Impact of TMEM2 on Stress Resistance Depends on p38 and ERK MAPK Signaling and Is Independent of JNK MAPK Signaling, Related to Figure 4

ER stress resistance of Wild-type, TMEM2-KO and CMV-TMEM2 overexpressing human fibroblast was measured in the presence of Tunicamycin (200ng/ml) and (**A**) the ERK inhibitor DEL-22379 (Concentration in bar graphs: DEL-22379 2μM), (**B**) the p38 MAPK pathway inhibitor SB239063 (Concentration in bar graphs: SB239063 50μM) or the (**C**) JNK MAPK pathway inhibitor AEG 3482 (Concentration in bar graphs: AEG 3482 100μM). Changes to Tunicamycin-induced ER stress resistance was determined through CTG analysis, after a 5 day treatment with 200ng/ml Tunicamycin; (n = 3) Statistical Analysis: One-way ANOVA analysis with post hoc Bonferroni-Holm analysis; * = p < 0.05; ** = p < 0.01, *** = p < 0.001. All bar graphs represent mean. All error bars for all plots represent standard deviation.
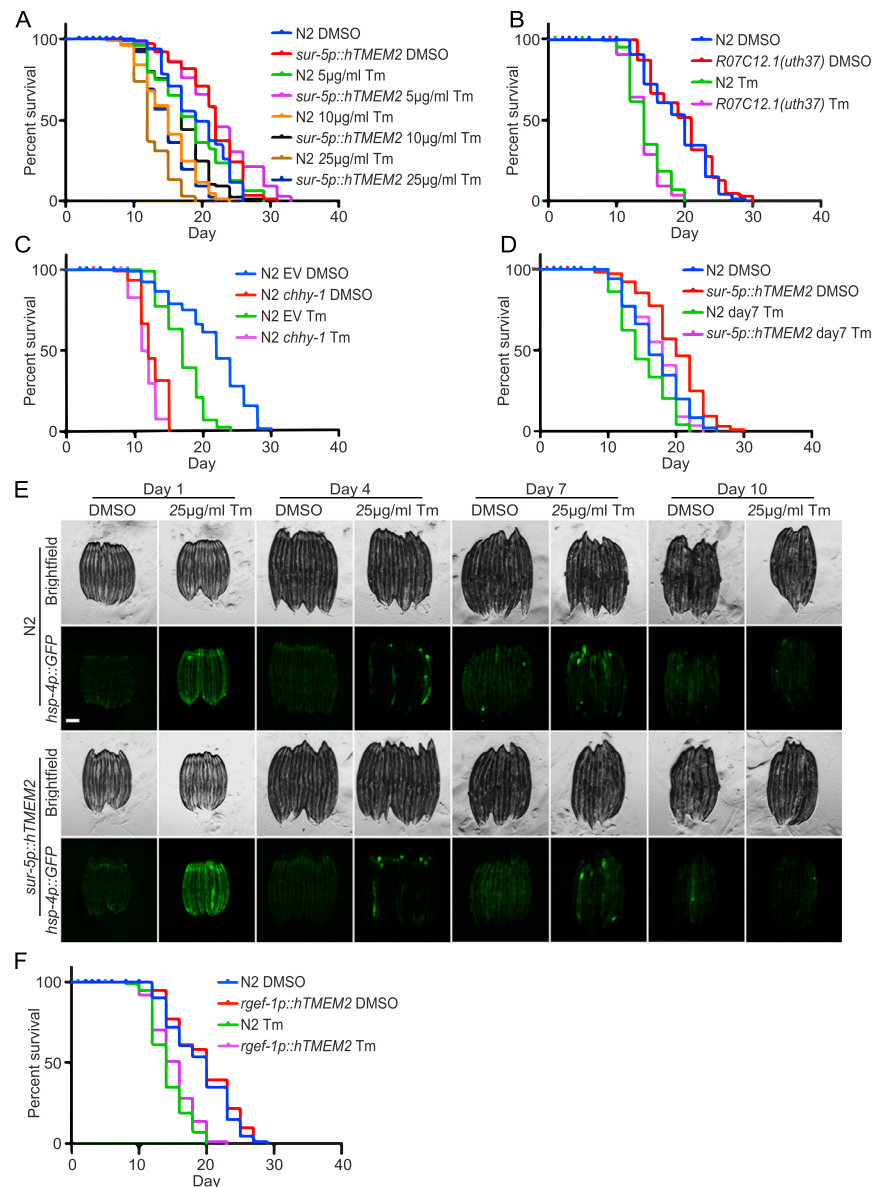
Figure S6. The Predicted *C. elegans* TMEM2 Homolog, *chhy-1*, but Not R07C12.1, Is Required for ER Stress Resistance, and Whole-Animal Overexpression of hTMEM2 Is Necessary for Lifespan Extension and Stress Resistance, Related to Figure 5

(**A**) Lifespans were measured in Wild-type (N2) and *sur-5p::hTMEM2* worms grown on EV RNAi on 1% DMSO, 5μg/ml, 10μg/ml, and 25μg/ml of Tunicamycin (Tm) from Day 1 (D1) as described in STAR Methods. Animals were developed on standard EV RNAi plates from hatch until D1. Data are representative of two independent trials. (**B**) Lifespan measurements of Wild-type (N2) or CRISPR-Cas9 null mutant *R07C12.1(uth37)* animals grown on EV RNAi on 1% DMSO and 25μg/ml Tunicamycin (Tm) from Day 1 (D1). Animals were developed on standard EV RNAi plates from hatch until D1. Data are representative of two independent trials. (**C**) Lifespan measurements of Wild-type (N2) animals grown on EV or *chhy-1* RNAi on 1% DMSO and 25μg/ml Tunicamycin (Tm) from Day 1 (D1). Animals were developed on standard EV RNAi plates from hatch until D1. Data are representative of two independent trials. (**D**) Lifespan measurements of Wild-type (N2) and *sur-5p::hTMEM2* worms grown on EV RNAi from hatch until D7. Animals were moved to either 1% DMSO or 25μg/ml Tunicamycin (Tm) at D7. Data are representative of three independent trials. (**E**) Fluorescent micrographs of Wild-type (N2) and *sur-5p::hTMEM2* animals expressing the UPR^{ER} reporter, *hsp-4p::GFP*. Animals were moved onto standard EV plates containing 1% DMSO or 25μg/ml Tunicamycin (Tm) 16 h prior to imaging – see STAR Methods for details. Data are representative of 3 independent trials. (**F**) Lifespan measurements of Wild-type (N2) or *rgef-1p::hTMEM2* animals grown on EV RNAi on 1% DMSO and 25μg/ml Tunicamycin (Tm) from Day 1 (D1). Animals were developed on standard EV RNAi plates from hatch until D1. Data are representative of three independent trials. All statistics for lifespans were performed using Log-Rank (Mantel-Cox) test using PRISM and are available in Table S2.
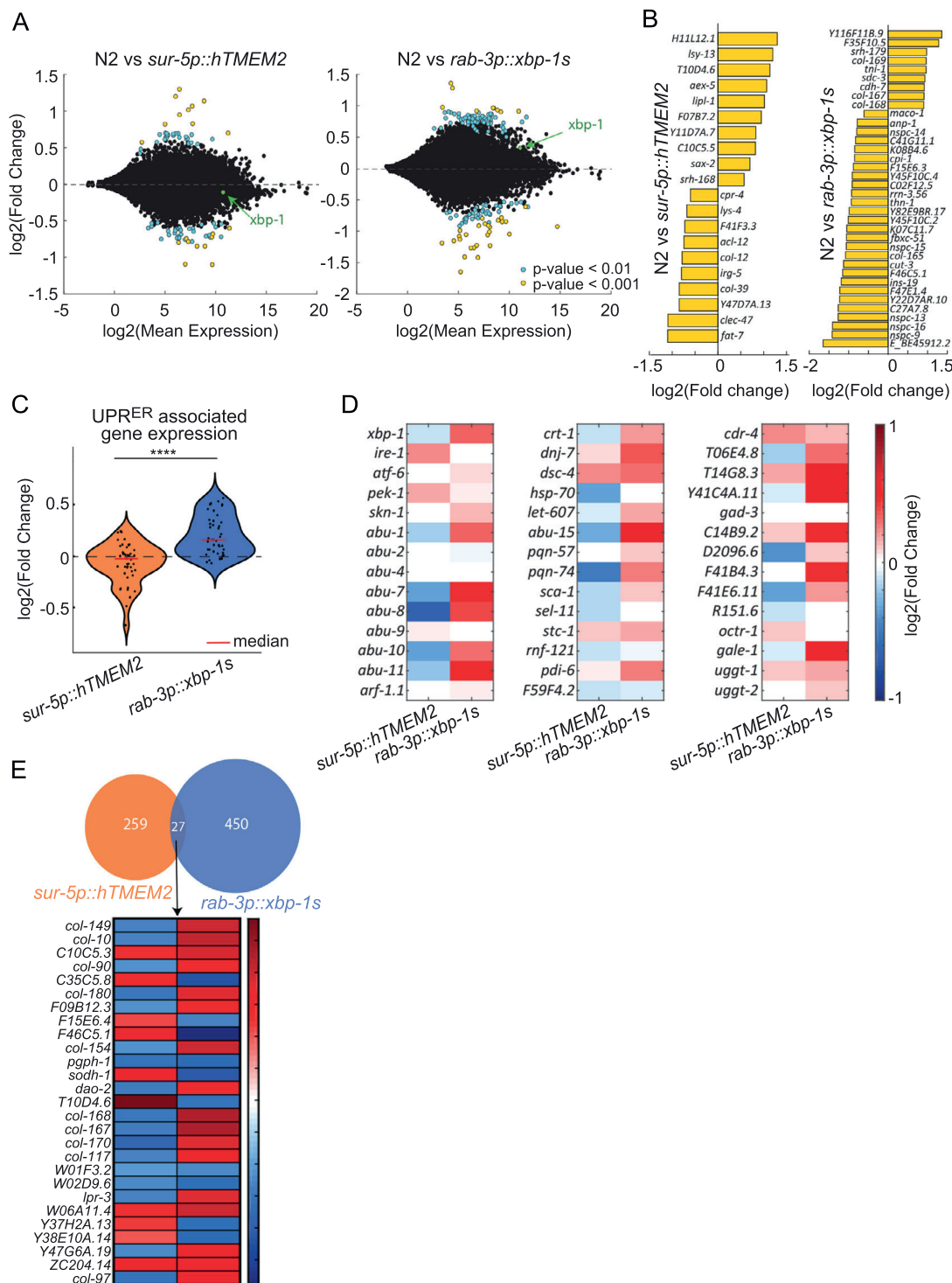
Figure S7. Overexpression of hTMEM2 in *C. elegans* Does Not Promote the Expression of Canonical UPR^ER Targets, Related to Figure 5

(**A**) RNA-sequencing was performed on Wild-type (N2), *rab-3p::xbp-1 s*, and *sur-5p::hTMEM2* animals. The log2-fold change in expression as a function of mean expression level is shown as compared to Wild-type. Genes are highlighted according to the significance of fold change (blue, p value < 0.01; yellow p value < 0.001). UPR^ER transcription factor, *xbp-1 s,* is highlighted in green. (**B**) Fold changes of the most significant changes (p value < 0.001) are plotted individually for *sur-5p::hTMEM2* (left) and *rab-3p::xbp-1 s* (right) animals compared to N2. Genes are non-overlapping. (**C**) Fold change of genes annotated

(legend continued on next page)

as UPR^{ER} (GO: 0030968) is shown. The median fold change is noted in a red line. The log2-fold change is also shown separately for each gene in (**D**). These data show that the UPR^{ER} is generally not activated in *sur-5p::hTMEM2* in comparison to *rab-3p::xbp-1 s* animals. (**E**) Venn diagram of significantly changing genes (p value < 0.05) (top). Fold-change of the 27 differentially expressed genes that are shared between the two strains (bottom). These data show that hTMEM2 and *xbp-1 s* overexpression result in distinct transcriptional changes.